INVESTIGATION OF THE HARDENING BEHAVIOUR AND ORDERING TRANSFORMATION IN Pt 14 at. % Cu

by

Muneeba Carelse

A dissertation submitted to the Faculty of Engineering and the Built Environment, University of Cape Town, in fulfilment of the degree of Master of Science in Applied Science.

Centre for Materials Engineering
Department of Mechanical Engineering

October 2005

ABSTRACT

The influence of prior cold work and quenching from elevated temperature on the hardening behaviour and ordering transformation in platinum 14 at. % copper has been investigated. Initially cold worked and initially quenched specimens were observed to increase in hardness upon heat treatment at temperatures between 100°C and 400°C. Additional superlattice reflections in electron diffraction patterns showed that an ordering transformation takes place in this alloy at these temperatures. The ordered structure which developed on heat treatment was identified as $CuPt_7$. Dark field imaging in the transmission electron microscope showed that small ordered regions nucleate during heat treatment but growth is very slow.

The degree of hardening after heat treatment was greater for the initially cold worked specimens than for the initially quenched specimens. Dark field images of initially cold worked specimens after heat treatment showed smaller ordered regions than the initially quenched specimens. This suggests that smaller, more numerous ordered regions impede dislocations to a greater degree than larger ordered regions in this alloy. The hardening mechanism thus appears to arise from dislocation impediment by the ordered regions.

Prolonged heat treatment of initially quenched specimens resulted in growth of the ordered regions to impingement and coalescence which was not seen in initially cold worked specimens. The observed difference in size and growth of ordered regions, and the consequent difference in hardening, can be accounted for by the vacancy concentration during heat treatment.

ACKNOWLEDGEMENTS

I would like to express my sincere thanks and appreciation to the following people:

- Professor Candy Lang, my SUPERvisor, for all her advice and encouragement throughout my degree.
- Professor Jannie Neethling and Miyelani Nzula with their help on the simulations.
- To Silethelwe, Chumani and everyone from the Centre for Materials Engineering, the best group of people one can only wish to work with.
- To Penny Park-Ross for her assistance with everything.
- To Glen Newins and Peter Jacobs for their assistance with the vacuum furnace and for making specimen holders.
- To Mohammed Jaffer and Sean Karriem from the Electron Microscope Unit at UCT for their assistance with the TEM.
- The financial support of the Innovation Fund is gratefully acknowledged.
- Finally, and most importantly to my family, for having faith in me and encouraging me throughout my life and this thesis.

CONTENTS

1 INTRODUCTION

Research into making stronger platinum jewellery alloys can be of great benefit to the platinum jewellery industry. Pure platinum is relatively soft and this limits design possibilities as well as making platinum jewellery prone to scratching and wear. Platinum containing 14 at. % copper is a widely used jewellery alloy because the copper confers solid solution strengthening to the relatively soft platinum. This copper concentration, at 5% by mass, meets international hallmarking requirements for platinum jewellery. In the jewellery industry it is known that heating of platinum 5 wt.% (14 at.%) copper can result in an increase in hardness and strength, but no systematic description of this phenomenon is available in the technical literature. Although ordering is known to influence hardness and strength, and ordering in platinum 14 at. % copper has been previously reported, the influence of ordering on the strength of this commercially important platinum-copper jewellery alloy has been neglected to date.

The effect of ordering on strength may be influenced by the rate at which the ordering process occurs and the number of defects present. In the current study, the influence of defects (introduced by deformation and by quenching from elevated temperatures) on hardness and on the kinetics of the ordering transformation in platinum 14 at. % copper is investigated. In order to evaluate the effect of composition on the hardening behaviour and the ordering process, platinum 14 at. % copper was compared to platinum 12.5 at. % copper.

The dissertation is outlined as follows. Chapter 2 focuses on the theory of order and phase stability as well as the effect ordering can have on mechanical properties of an alloy system. The platinum copper alloy system as predicted by its equilibrium phase diagram is explained and a detailed description is given of previous work done on platinum copper alloys. Chapter 3 gives the experimental procedure followed throughout this investigation of the platinum 14 at.% copper alloy. Results presented in Chapter 4 include mechanical properties, x-ray diffraction analysis, light microscopy and transmission electron microscopy. Chapter 5 discusses the results and interprets the structure analysis whilst in Chapter 6 the conclusions drawn from the research work are presented. Chapter 7 contains proposals for future work.

2 LITERATURE REVIEW

2.1 SUPERLATTICE FORMATION

A solid solution is formed when atoms of two or more elements are able to share together, in changing proportions, various sites of a given crystal structure[1]. There are a number of different ways in which two elements in a binary solid solution can be arranged[2]. The most common is the almost random distribution, where statistical preferences for like or unlike nearest neighbours are certain to be present[2]. Another major group of alloys is one where the different atoms are located on distinct lattice sites and these retain their configuration right up to the melting point[2]. Such alloys occur at or near stoichiometric compositions and are called intermetallic compounds[2]. Another category of alloys are those which fall in between the atomic classifications of intermetallics and random solid solutions. This group depends on a sharply defined critical temperature, known as the critical ordering temperature (T_c)[2]. Below T_c the atoms have a strong preference for specific lattice sites, while above this temperature a random solid solution is present although small groups of unlike nearest neighbours (short range order) are found to exist[2]. These alloys fall into the group of ordered alloys. The ordered structure which forms below T_c is commonly known as a superlattice or superstructure[2].

The majority of typical superlattices are related to the three principal metallic structures, the face centred cubic (A1), the body centred cubic (A2) and the close packed hexagonal (A3). It is becoming a generally accepted practice to refer to

specific superlattice types by their Strukturbericht designations. Examples of superlattice structures are given below.

Alloy	Strukturbericht Designation
Cu_3Au type structure	$L1_2$
CuPt type structure	$L1_1$
CuAu type structure	$L1_0$

Table 2-1 Common types of superlattices and their Strukturbericht designations (after Barrett and Massalski[1]).

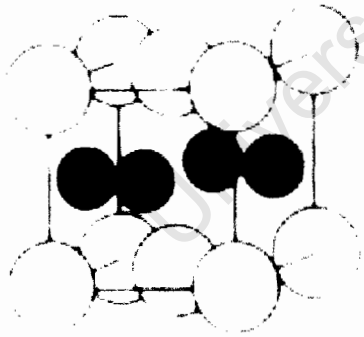

a) CuAu / $L1_0$

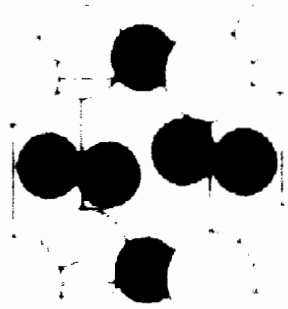

b) Cu_3Au / $L1_2$

Figure 2-1 Examples of the CuAu and Cu_3Au superlattice structures (after Barrett and Massalski[1]).

2.2 ORDERED ALLOYS

Ordering is a process whereby atomic arrangement in a crystal lattice changes from a random to a more ordered state. In the ordered arrangement, certain lattice sites are occupied predominantly by the same type of atom. A disordered arrangement of atoms in an alloy of AB composition occurs when either A or B can occupy any given site. On ordering of the AB alloy, the atoms A and B start to segregate and show some kind of preference for particular lattice points. The resultant structure can be described as a lattice of A atoms interpenetrating a lattice of B atoms[1]. An example of this type of lattice is the Cu_3Au alloy. Figure 2-2 shows the disordered lattice, where copper and gold atoms can occupy any of the atomic sites as long as Au:Cu remains 1:3, and the ordered lattice, which has preferred atomic sites for copper and gold atoms[1].

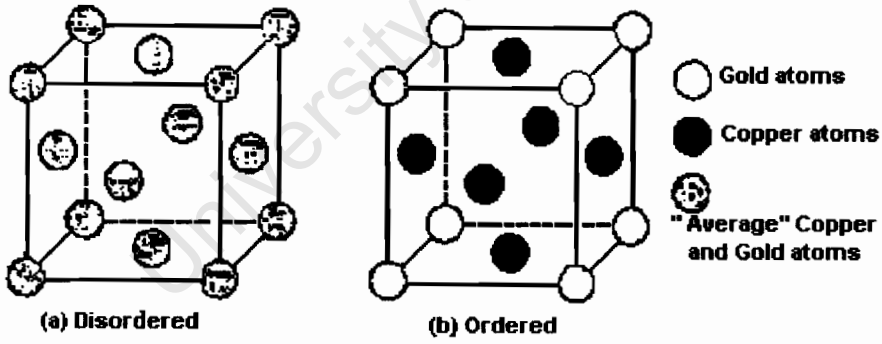

Figure 2-2 Unit cell of disordered and ordered Cu_3Au (after Barrett and Massalski[1]).

2.2.1 LONG RANGE ORDERING

In a fully ordered alloy there are directions within a crystal along which there is a perfect arrangement of A atoms on one set of lattice points and B atoms on another set. The ordering is consistent through long distances. The degree of this long range order is given by the long range order parameter S, which is defined as,

$$S = \frac{p - r}{1 - r} \qquad \textbf{Equation 1}^{1}$$

where p is the probability that an A atom site is filled by an A atom, and r is the fraction of the total sites that are occupied by A atoms for perfect order. S varies from 0 for disorder to 1 for full order[1]. Long range ordering takes place at relatively low temperatures compared to the melting temperatures, at or near simple stoichiometric compositions like A_3B, AB, AB_4, etc. The amount of order present within a material increases from zero at T_c to almost perfection at low temperatures[2].

2.2.2 SHORT RANGE ORDERING

Solid solution alloys that form superlattices are particularly likely to exhibit short-range order (SRO) at temperatures above T_c. This ordering can be retained at low temperatures by rapid quenching from above T_c. Short range order is defined in terms of the number of 'right pairs' of atoms, just as long range order is defined in terms of the number of right atoms on a given sublattice. A right pair is a pair of unlike atoms, an AB pair. At increasing temperatures the number of AB pairs diminishes and the number of AA and BB pairs (wrong pairs) increases[3].

Short range order can also occur below T_c, before full order is attained or at off-stoichiometric compositions. Research to date has led to the development of mainly

four models of short range ordering: statistical short range order, disperse short range order, microdomain short range order and the lattice defect model. These models are discussed in more detail below.

2.2.2.1 THE STATISTICAL SHORT RANGE ORDER MODEL

In this model, a one phase state of equilibrium is considered, i.e. short range order is homogeneous[3]. The Warren-Cowley SRO parameters α_i are appropriate to describe this type of microstructure and can be defined as:

$$\alpha_i = \varepsilon_i \frac{(X_a - X_b)^2}{1-(X_a - X_b)^2} \qquad \textbf{Equation 2}^{4}$$

where α_i is the probability of finding a B-atom in the ith coordination sphere around an A-atom independent of the special lattice point, ε_i is the correlation function, X_a is the atomic fraction of atom A and X_b is the atomic fraction of atom B. The described SRO is homogenous through out the crystal[4]. This type of SRO is typically observed at temperatures above T_c.

2.2.2.2 THE DISPERSE SHORT RANGE ORDER MODEL

In this model, a two phase state of equilibrium is considered, i.e. short range order is heterogeneous[3]. The fluctuations in concentration and in the degree of order are no longer statistical. One may define disperse short range order as dispersely distributed particles of a long range ordered phase in a less ordered matrix[3]. A special feature of this model is the fact that the ordered particle size increases and then remains constant at a value that is characteristic for each system. The special

conditions which can lead to the stabilisation of such a finely dispersed, two-phase state are determined by the coherence of the phase boundaries and the associated degree of order[5]. This type of order can occur for temperatures below T_c and off-stoichiometric compositions.

2.2.2.3 THE MICRODOMAIN SHORT RANGE ORDER MODEL

In this model, a heterogeneous type of short range order is considered, consisting of relatively well-defined and well-ordered regions (the microdomains) embedded in a random matrix. Only the degree of order varies between the microdomains and the matrix, not the composition[3]. This type of short range order occurs below T_c, at the stoichiometric composition.

2.2.2.4 THE LATTICE DEFECT ORDER MODEL

This model refers to metastable states where short range order is heterogeneous and compositional variations arise because of lattice defects such as quenched-in vacancies or dislocations introduced by plastic deformation[3]. In this model it is assumed that a higher degree of order occurs in the presence of lattice imperfections, while the lower degree of order corresponds to the matrix which does not contain much distortion. The degree of order present in the system is hence stabilized by dislocations and lattice defects[4].

The process of ordering depends largely on the mechanism of ordering as well as the kinetics of the transformation. These concepts are discussed in Section 2.3 and 2.4 respectively. The existence of local order (short- or long-range) has been associated

with changes in the mechanical properties of alloys. This type of strengthening is called long range order hardening or short range order hardening, depending on the degree of order present in the alloy. Strengthening of ordered alloys is discussed in Section 2.6.

2.3 MECHANISMS OF SUPERLATTICE FORMATION

The transformation characteristics of a previously disordered alloy when heated below the critical ordering temperature depend on the ordering mechanisms which are operative as equilibrium is approached[2]. An ordering mechanism cannot be deduced from the equilibrium state. The mechanism is selected from a number of possible alternative ordering mechanisms[2]. Even though the ordering transformation is thermodynamically possible, the ordering mechanism that will operate is the one that has the lowest activation energy barrier[2].

There are two main types of ordering mechanisms. Drastic atomic rearrangements within very small localised volumes are termed Type I transformations (nucleation and growth), while very small atomic rearrangements spread over large volumes are termed Type II transformations (homogeneous reaction).

2.3.1 TYPE 1 TRANSFORMATION

In this type of transformation, small ordered regions are nucleated at random points within the sample and these centres then grow at the expense of the disordered phase, by independent transference of atoms at the boundary[2]. At times, the new phase grows at sites where preferential nucleation had previously taken place[2]. By convention, heterogeneous nucleation is described as growth starting at specific sites such as grain-boundaries, dislocations etc., but in the realm of an ordering transition, a heterogeneous reaction refers to a transformation in discrete localised regions that is not necessarily at sites of crystal imperfections[2].

2.3.2 TYPE II TRANSFORMATION

In this type of transformation, annealing below the critical ordering temperature results in the superlattice forming at all points in the sample[2]. The degree of order increases upon isothermal annealing and disordered and ordered regime do not exist side by side. Under equilibrium conditions, the lattice would be indistinguishable from that obtained from Type I transformation, but the transient manifestations are totally different[2].

In some alloys the ordering reaction cannot be categorized as either Type I or Type II. Cu_3Au is an example of a Type I reaction but ordering can also occur homogeneously (Type II) in this alloy when the annealing temperature is lowered[6]. In another example, Fe_3Al orders homogeneously on continued cooling (Type II), and orders isothermally by nucleation and growth (Type I)[6].

2.4 KINETICS OF SUPERLATTICE FORMATIONS

Kinetics play a central role in the study of ordering transformations. Factors such as temperature, defects and composition of the alloy can affect the ordering kinetics. These factors are discussed below.

2.4.1 TEMPERATURE

An ordering transformation is dependent on the temperature of the heat treatment which must allow for atomic diffusion and hence superlattice formation[7,8].

Electrical resistivity has generally been utilised to follow the change in ordering kinetics and degree of order during heat treatment[7]. At low temperatures, resistivity usually remains constant due to the concentration and/or mobility of vacancies being unable to facilitate ordering kinetics[7]. With increasing temperature the increase in mobility of vacancies allows the ordering process to start and a corresponding decrease in the electrical resistivity is observed until the equilibrium degree of order is reached at the resistivity minimum[7].

The quality of the quenching procedure before the isothermal annealing may also affect ordering kinetics. If the initial quench was fast enough, the ordering kinetics will increase. A significant amount of ordering occurred in Au-14 at. % Fe after quenching from between 543K and 573K followed by isothermal heat treatment at 473K[8]. Migschitz *et al.*[8] attributed this increased kinetics to higher quenching temperatures that introduced an increased number of quenched in vacancies needed for ordering to occur.

2.4.2 DEFECTS

Defects can be created by irradiation, by quenching from high temperatures, or by plastic deformation[9]. Irradiation creates equal numbers of interstitials and vacancies; quenching involves predominantly the production of only vacancies; plastic deformation introduces a variety of defects, including interstitials, vacancies, dislocations, jogs and stacking-faults[9].

The effects of deformation and recrystallisation on SRO kinetics studied in Fe-Pd showed that deformed samples exhibited markedly increased ordering kinetics compared to undeformed samples[10]. The resistivity of deformed Fe-Pd decreased rapidly on heating as seen in Figure 2-3, so that it reached equilibrium order (minimum of resistivity curve) at a lower temperature than the undeformed sample[10]. Kulovits *et al.*[10] ascribed this difference in ordering behaviour to the high internal stresses produced by deformation, which induces preferential domain alignment resulting in a higher degree of order in the deformed specimens. Dislocations were favourable nucleation sites for ordered domains, resulting in faster and coarser precipitation of the new ordered phase[10,11].

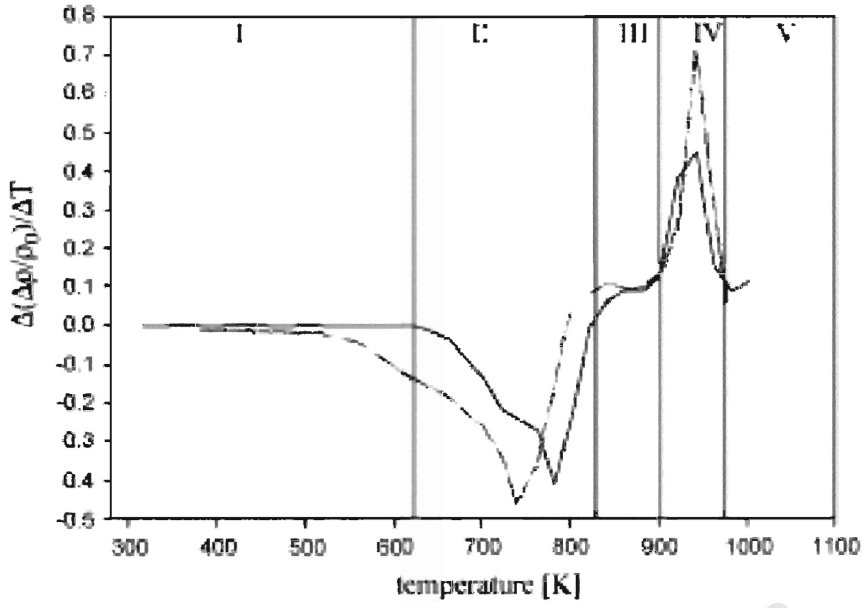

Figure 2-3 Differentiated relative resistivity change of the forward isochronal runs vs temperature. Dashed line: deformed Fe-Pd sample, full line: undeformed Fe-Pd sample (after Kulovits *et al.*[10]).

There are however opposing views regarding the effect of deformation on the ordering kinetics and the degree of order in an alloy system. On the one hand, vacancies produced by deformation have a positive affect on ordering kinetics and the degree of order[10,11]. On the other hand, deformation can also have a negative affect on the ordering kinetics and the degree of long range order by producing vacancy sinks, eg. dislocations[12,13,14]. Even though deformation produces a high concentration of vacancies needed for the ordering transformation to occur, these vacancies can be annihilated at dislocations resulting in a decrease in ordering kinetics[15,16]. Introducing plastic deformation in some alloy systems resulted in a decrease in the degree of order[10-16]. Furthermore, the interaction between dislocations and solute atoms can result in a solute flux to dislocations, therefore a lower solute fraction is available for precipitation of a new phase[17,18]. Given this variety of possible interactions, the effect

of dislocations on ordering kinetics and the degree of order strongly depends on the alloy family and ageing sequence.

2.4.3 COMPOSITION

The composition within an alloy system has been shown to affect ordering kinetics. The rate at which short range order in α-CuAl is reached is reported to increase with increasing aluminium content as shown by the resistivity minima in Figure 2-4. The reason for the slower ordering kinetics of α-CuAl alloys with lower aluminium content was due to the type of short range order occurring in the alloy upon heat treatment[4]. The ordering type in Cu 10 at. % Al and Cu 15 at. % Al was best interpreted as disperse short range order[4]. This type of order occurs at a slower rate because the adjustment of a new number of precipitated domains takes more time, i.e. atoms have longer diffusion paths[4]. At high aluminium concentrations disperse short range order changed into the microdomain structure, where the volume fraction of ordered domains was much larger[4]. This allows for shorter diffusion paths and hence faster ordering kinetics [4].

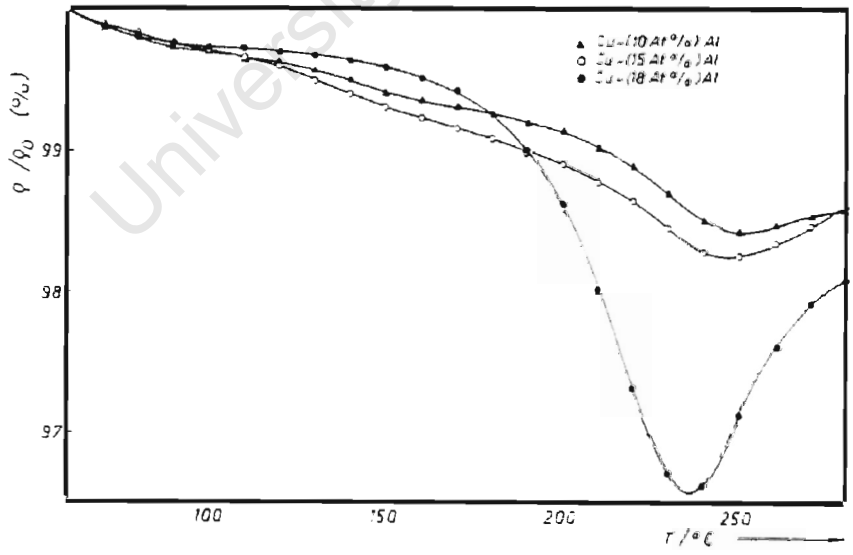

Figure 2-4 Resistivity curve of Cu-10/15/18 at.% Al demonstrating the resistivity minimum increase with increasing Al concentration (after Trieb and Veith[4]).

Studies done on ordering kinetics in Cu-Mn showed a different trend to that seen for Cu-Al. In the Cu-Mn alloys, equilibrium short range order was reached fastest for Cu-13 at. % Mn, followed by Cu-16, Cu-8, Cu-20 and Cu-5 at. % Mn[19]. Reishner and Pfeiler[19] were unable to distinguish between the various interpretations for short range order types occuring at the different compositions. However, they attributed the fast ordering kinetics to the maximum atomic mobility occurring at Cu 13 at. % Mn which was correlated with the increased interaction energies of the first and second nearest neighbour atoms[19].

2.5 THE PLATINUM COPPER SYSTEM

Copper and platinum are known to form a continuous solid solution in the whole composition range, as shown in Figure 2-5. At low temperatures copper platinum alloys undergo a disorder-order transition into long range ordered structures where different types of ordered structures form depending on the alloy composition.

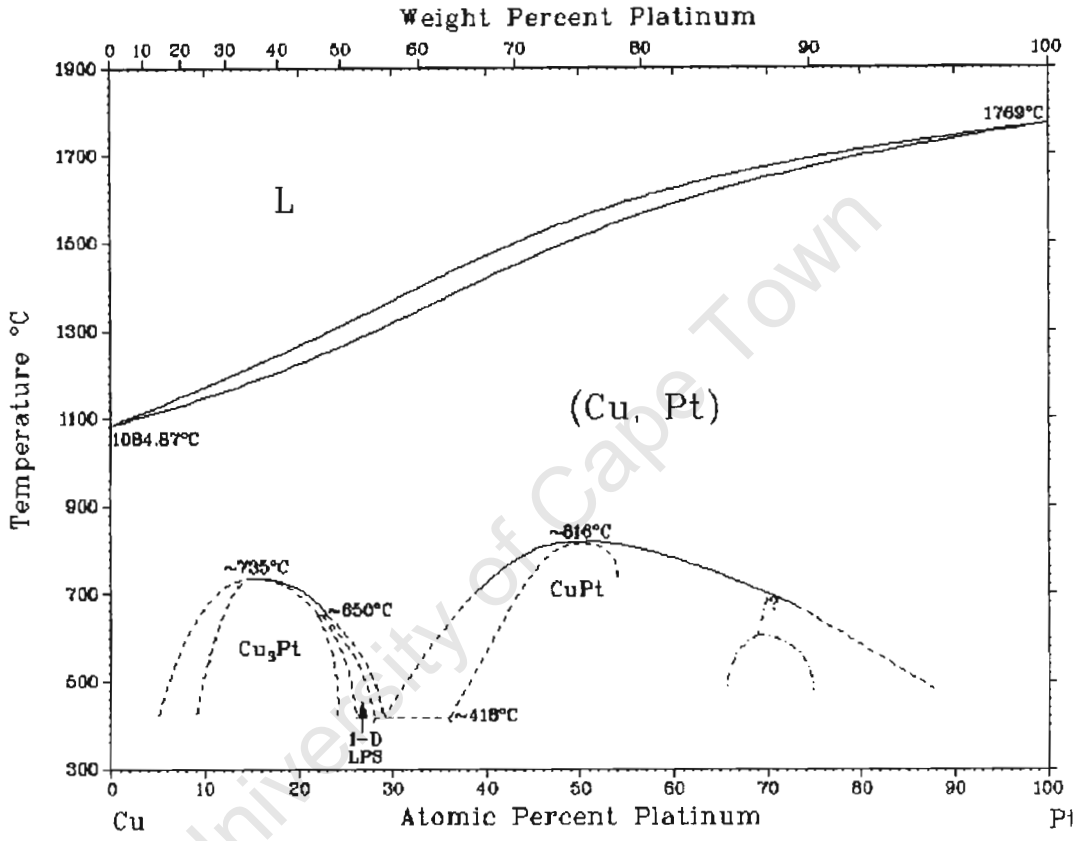

Figure 2-5 Platinum copper equilibrium phase diagram (after ASM International: Binary Phase diagrams[20]).

The existence of three ordered phases, Cu_3Pt, CuPt and $CuPt_3$ has been established[21]. In alloys with more than 24 at.% Pt, a periodic one-dimensional anti-phase domain structure based on a face-centered tetragonal cell with atomic arrangement of the ordered Cu_3Au type appears in the limited temperature range immediately below the

critical ordering temperature T_c, although the $L1_2$-type structure is stable at lower temperatures. The alloys in the Cu_3Pt region with Pt less than 24 at.% have the $L1_2$-type structure in the whole temperature range below T_c[21].

The equiatomic CuPt has been very well researched due to the unusual superlattice structure that forms during ordering. CuPt exists such that alternate layers of pure copper and platinum atoms arrange themselves parallel to the (111) planes[22]. The resulting symmetry of the crystal is a rhombohedral superstructure of the $L1_1$-type and the original cubic lattice is slightly distorted in the [111] direction. This is illustrated in Figure 2-6. The CuPt ordered phase was found to exist in a wide composition range centered at 50 at.% Pt[22].

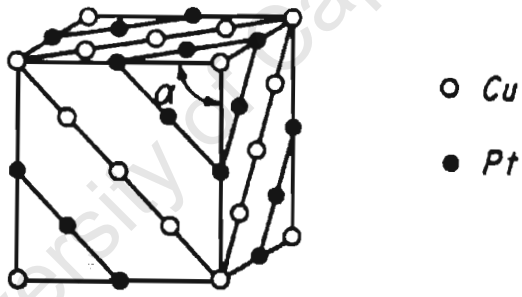

Figure 2-6 Atomic arrangement of the ordered structure of CuPt (after Wu *et al.*[22]).

The existence of other superlattice structures has also been reported in the platinum rich region. Two possible ordered structures formed at compositions near $CuPt_3$ have been suggested. Schneider and Esch[23] proposed an orthorhombic structure, which is derived from a face centered cubic arrangement. This phase has two kinds of (111) layers stacked alternately, one consisting of platinum atoms and the other of copper and platinum atoms arranged regularly along the (1-11) direction. This structure is

shown in Figure 2-7a. A second type was suggested by Tang[24], who pointed out the inconsistency of Schneider and Esch's results on $CuPt_3$. It is thought by Tang that the orthorhombic structure suggested by Schneider and Esch would probably distort the cubic lattice perceptibly, yet no splitting of the diffraction lines was observed in their results[24]. Tang found a different structure model for $CuPt_3$, which gave an intensity distribution in good agreement with the observed one[24]. Figure 2-7b shows the Tang structure type with cubic symmetry.

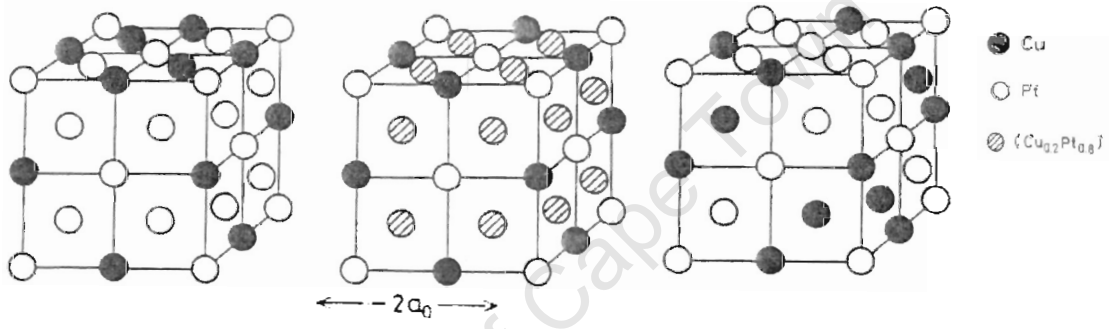

a) $CuPt_3$ orthorhombic **b) $CuPt_3$ cubic** **c) Cu_3Pt_5**

Figure 2-7 Structure types of Cu-Pt superlattices (after Miida and Watanabe[25]).

Miida and Watanabe[25] followed up on Tang's work and studied Cu-Pt alloys around composition $CuPt_3$ by using electron microscope and diffraction studies. They were able to show that below the order-disorder transformation temperatures three structure types exist, as shown in Figure 2-7 above. A rhombohedral lattice of Cu_3Pt_5 (Figure 2-7c) exists in alloys containing less than 70 at. % Pt while in alloys containing more than 70 at. % Pt the $CuPt_3$ type superlattice exists[25]. At temperatures below 600°C the orthorhombic $CuPt_3$ type superlattice is stable in the composition range of approximately 68 - 75 at. % Pt [25]. Figure 2-8 shows the partial phase diagram around composition $CuPt_3$ as determined by Miida and Watanabe[25].

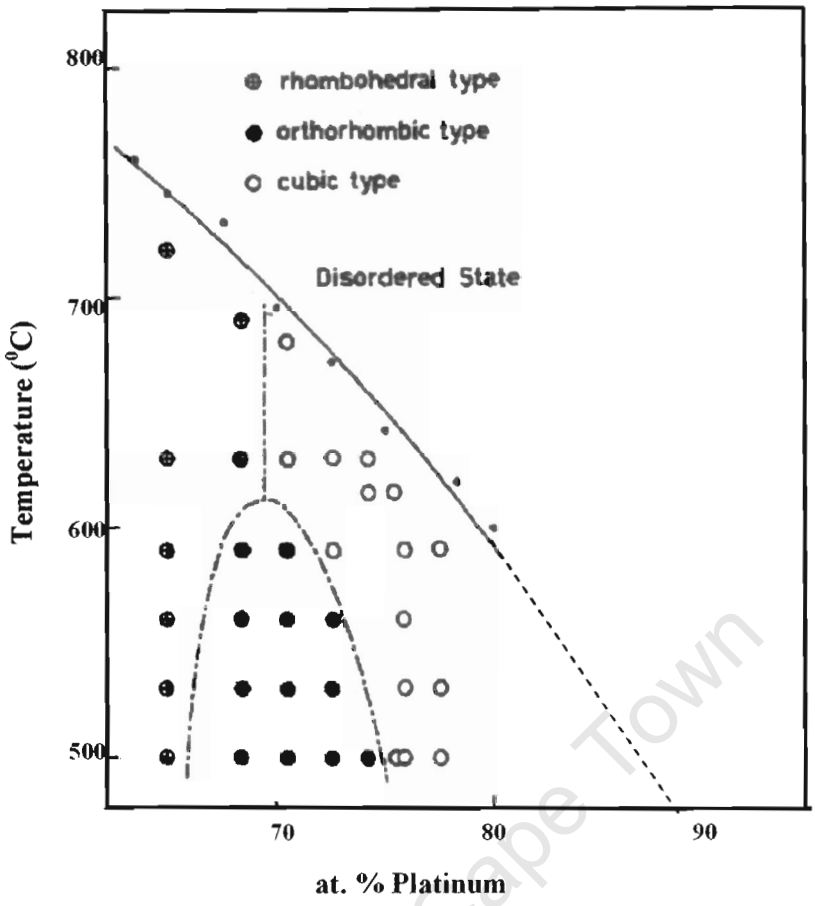

Figure 2-8 The partial phase diagram around the composition $CuPt_3$. Small circles represent critical ordering temperatures (after Miida and Watanabe[25]).

The platinum copper alloy with the lowest copper concentration reported to date is at composition 87.5 at. % Pt ($CuPt_7$). X-ray diffraction studies done by Saha *et al.*[26] on the Cu-87.5 at.% Pt alloy showed that ordering occurs at temperatures below 430°C. Tang's model has previously been used by Miida and Watanabe[25] to explain the ordered structure of the Cu-78 at.% Pt alloy. Saha *et al.*[26] then assumed that the stable region of the ordered structure extends from 75 at.% Pt to 87.5 at.% Pt and adopted Tang's model (Figure 2-7b) as the ordered structure forming at Cu 87.5 at. % Pt.

Tang's model is better known as the ABC_6 ordered structure and is stable over the platinum range 68 at. % Pt to 88 at. % Pt[24]. The structure has a unit cell which is 2×2×2 as large as that of the fundamental fcc structure, with the A-sites occupied by Pt atoms, the B-sites by Cu atoms and the C-sites by the remaining atoms statistically according to composition[24]. The percentage of Pt or Cu atoms taking up the C atomic site can be given by,

$$(Pt_{1-x}\,Cu_x)\,(Pt_y\,Cu_{1-y})\,(Pt_{1-z}\,Cu_z)_6 \qquad \textbf{Equation 3}$$

where the composition of the platinum copper alloy is given by,

$$\textbf{at. \% Pt} = [100\,(7 - x + y - 6z)] / 8 \qquad \textbf{Equation 4}$$

where x, y and z are arbitrary numbers less than 0.3.

At the composition Cu 86 at. % Pt , (x,y,z) is equal to (0,0,0.02) and equation 3 becomes $(Pt)(Cu)(Pt_{0.98}Cu_{0.02})_6$. If (x,y,z) is equal to (0,0,0), the structure in equation 3 becomes $(Pt)(Cu)(Pt)_6 \equiv CuPt_7$, and all C sites are thus taken up by Pt atoms. At this composition (87.5 at. % Pt), Tang's model becomes Schneider-Esch Model[23] as illustrated in Figure 2-9.

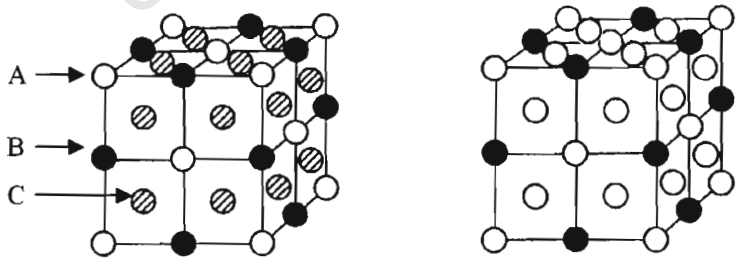

(a) **(b)**

Figure 2-9 (a) Tang's model (ABC_6 structure) and (b) Schneider and Esch's model (A_7B structure) (after Tang[24] and Schneider and Esch[23]).

The same structure formed at $CuPt_7$ forms at the composition Cu_7Pt and was determined experimentally by x-ray diffraction as well as theoretically using the Monte Carlo simulation[27]. Takizawa *et al.*[27] theoretically predicted that the double-sized fcc structure is the most stable phase occuring at Cu_7Pt. The Cu_7Pt structure studied by Takizawa was to be taken as a super-structure on the $L1_2$ structure[27]. This idea of secondary ordering was developed by Khachaturyan[28] in his theory of the concentration wave model for ordering in a binary alloy. Tang's model can be understood as a secondary structure forming in the $L1_2$ phase field. It was found by Takashi *et al.*[29] that the Tang model forms in the Pt-Mn system at compositions between 12.5 at.% Mn and 14 at.% Mn. The structure forms through a double-step ordering sequence, disordered FCC→ $L1_2$→ Tang model[29]. This type of secondary ordering has not been observed in the platinum rich region of the Pt-Cu system, where instead Tang's model forms directly from the disordered FCC lattice[26].

It was pointed out by Men *et al.*[30] that at least interactions up to the third-nearest neighbour are necessary to stabilize Tang's Model. Saha *et al.*[26] concluded that a thermodynamical treatment will need to introduce more long-range interactions than those of the nearest and next-nearest neighbours if any interpretations of different structural changes were to be made.

2.6 ORDER STRENGTHENING

Order strengthening is the term used to describe the increased strength of an alloy after undergoing an ordering transformation[6]. The degree of ordering can have a large effect on the mechanical behaviour of an alloy, i.e. the strength changes as the alloy changes from a disordered to an ordered state[6]. The degree of order is given by the long range order parameter S, which is defined in Section 2.1. This section will discuss how the magnitude of the long range order parameter affects the mechanical properties of an alloy.

2.6.1 INTERMEDIATE DEGREE OF ORDER (S~0.5)

Strength is at a maximum in the partially ordered state and a system such as Fe_3Al is an example of this[6]. Figure 2-10 and Figure 2-11 show a maximum in flow stress of Fe_3Al occurring when S is approximately 0.5, where flow stress was measured at elevated temperatures or room temperature.

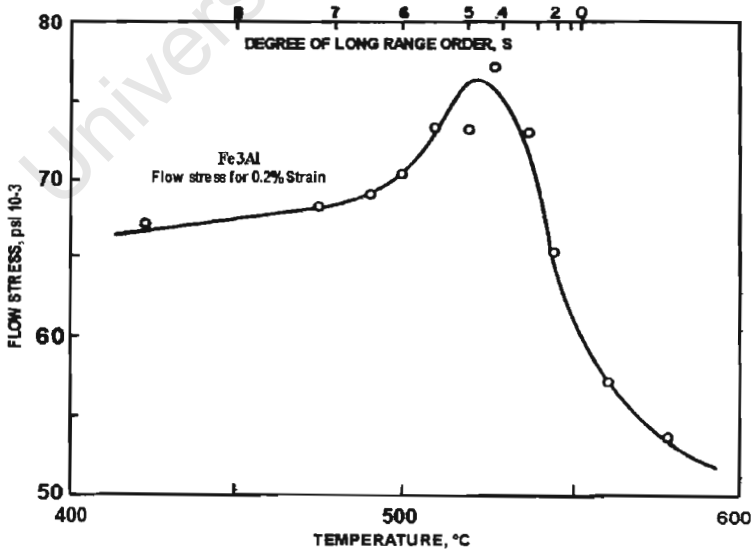

Figure 2-10 The dependence of the flow stress of Fe_3Al on the degree of long range order tested at elevated temperatures (after Stoloff and Davies[6]).

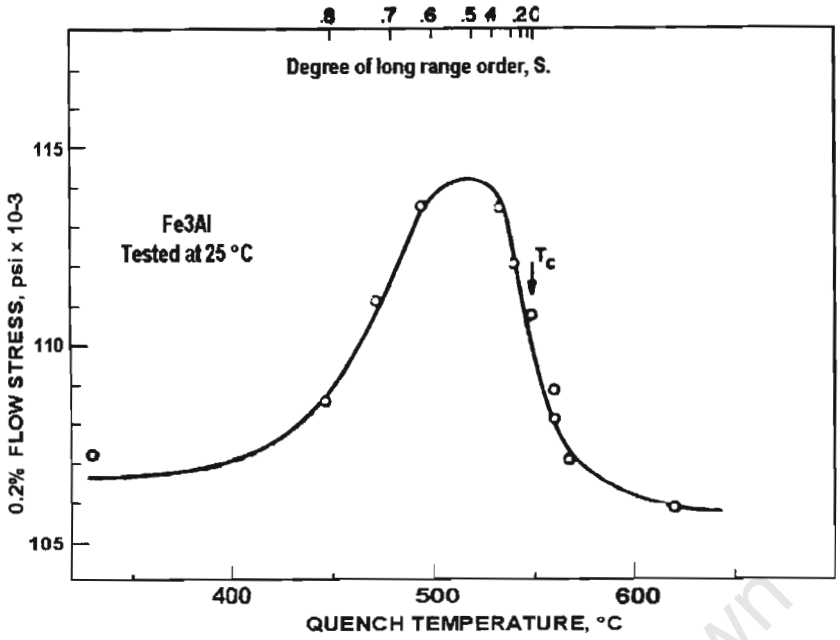

Figure 2-11 The dependence of the flow stress of Fe_3Al on the degree of long range order tested at 25°C (after Stoloff and Davies[6]).

Stoloff[6] proposed a theory to explain variations in flow stress below T_c, by considering the variation in spacing between dislocation pairs and the change in the degree of order. The dislocation spacing is inversely proportional to S^2. If S is low, superlattice dislocations dissociate into their unit dislocations, which can glide independently. Unit dislocations in an ordered alloy leave antiphase boundary trails, thus creating wrong bonds which give rise to the hardening. As S increases, unit dislocations associate in pairs. The superlattice dislocations glide in the ordered matrix and create, on average, no wrong bonds. The strength will begin to decrease as the proportion of superlattice dislocations increases. A drop in the flow stress is to be expected when a large proportion of dislocations are gliding in pairs, and the flow stress will continue to decrease with increasing order. Stoloff[6] concluded that a peak in strength will be observed at some intermediate degree of order for materials in which the degree of order varies from 0 to 1.

Alloys that consist of perfectly ordered regions in a disordered matrix can also be said to display an intermediate degree of order. Some partially ordered alloys also exhibited strengthening after isothermal annealing[31,32,33]. These partially ordered alloys were two phase structures consisting of either ordered plus disordered or ordered plus short range ordered regions. The partially ordered alloys can either be in an equilibrium or non-equilibrium state, where in the latter state ordered domains grow up to impingement[31,32,33]. Different strengthening mechanisms proposed for partially ordered alloys are discussed in the following paragraphs.

'Short range order strengthening' was the reason for the retained hardness of Ni_3Fe and Ni_3Mn[31]. In this strengthening mechanism superlattice dislocations present in the ordered and short range ordered structure moved easily through the ordered domains and needed extra stress to overcome the resistance offered by the short range ordered regions. As the domains grew the volume of the short range ordered material decreased and the strength continued to increase[31]. This was explained by the faster increasing degree of short range order compared to the decrease in volume fraction of the short-range ordered materials[31].

Another proposed strengthening mechanism present in some alloys was 'domain hardening'. In Cu_3Au and Mg_3Cd, the softening occurring after prolonged heat treatment was explained by the method originally proposed by Cottrell[34] and Flinn[35]. Figure 2-12 shows that the strength of the alloy decreases from the maximum hardness reached at a domain size of 40 Å. Stoloff and Davies[31] showed that at this domain size, an intermediate degree of order is obtained and at domain sizes more than 100 Å, the degree of order becomes constant; i.e. the alloy reaches an

equilibrium degree of order where S~0.8 (Figure 2-13). In this fully ordered condition, the dislocations move in pairs and this creates only a small amount of antiphase boundary. Movement of dislocations through fully ordered domains does not require as much energy as the partially ordered structure[31]. This results in a drop in hardness.

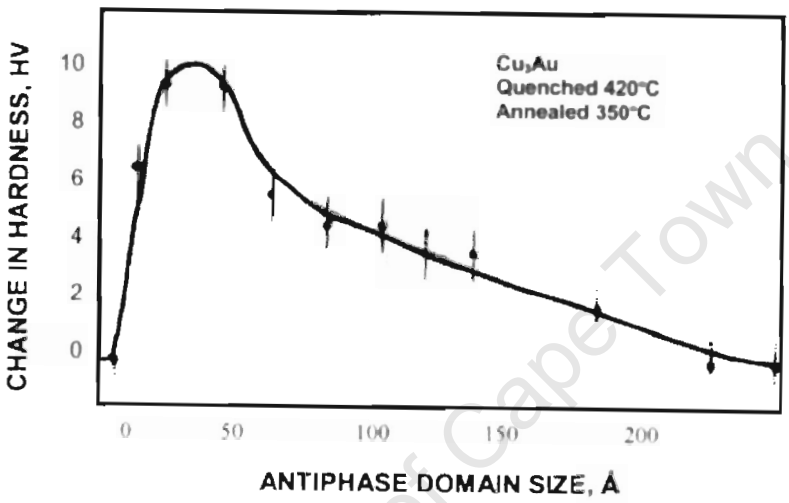

Figure 2-12 Change in hardness with domain size for Cu_3Au (after Stoloff and Davies[31]).

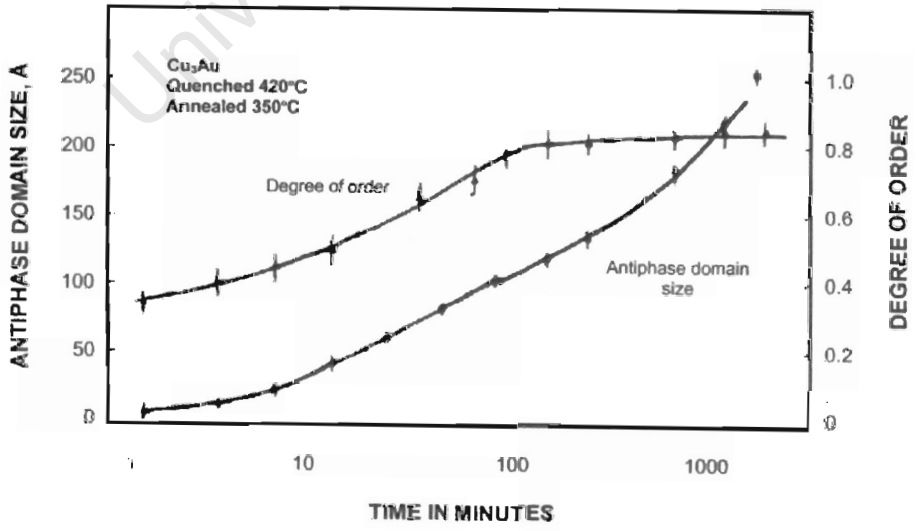

Figure 2-13 Kinetics of ordering and domain growth for Cu_3Au upon annealing at 350°C (after Stoloff and Davies[31]).

2.6.2 PERFECT LONG RANGE ORDER ($S = 1$) AND COMPLETE DISORDER ($S = 0$)

Quenched Ni_4Mo showed maximum hardness as perfect long range order was achieved and as the domain size increased after prolonged heat treatment (see Figure 2-14)[13]. In alloy systems such as Cu_3Au and Mg_3Cd, progressive softening occurs with an increased value of S and domain size after prolonged heat treatment[31,32]. The influence of perfect order on strength therefore varies between different alloys.

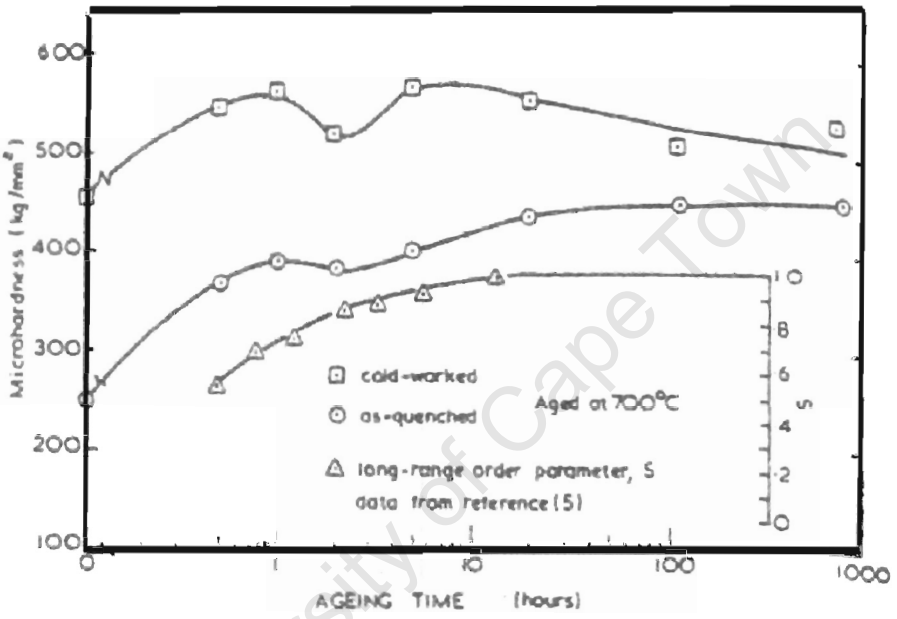

Figure 2-14 Microhardness variations as a function of ageing time for Ni_4Mo annealed at 700°C (after Ling *et al.*[13]).

The strengthening mechanism associated with an ordering reaction in systems such as Ni_4Mo has been described by Irani and Cahn[36]. Here the strengthening was attributed to a combination of small domain size and coherency stresses generated during the transformation. It has been proposed that Ni_4Mo retains its high strength on continued annealing because the growing domains remain coherent even though they are highly strained[37]. Large ordered grains in Ni_4Mo contain a multitude of small domains which have developed as a result of a stress-relief mechanism that relieves

internal strains, accompanying the ordering reaction. These domains can be thought of as being "pseudo recrystallised grains" and their formation has been observed in several other ordered alloys[38].

The strength of the as-quenched and fully ordered materials differs greatly when tested at elevated temperatures[6]. Figure 2-10 shows that testing done at elevated temperatures on Fe_3Al resulted in a higher strength of the fully ordered alloy compared to the as-quenched alloy. This is due to the onset of diffusion occuring at elevated temperatures and the as-quenched specimens do not retain their order during testing whereas fully ordered specimens do[6]. At room temperature however, there is not much difference between the strength of as-quenched and ordered Fe_3Al as shown in Figure 2-11. For samples tested at room temperature, the as-quenched specimens retain their order, hence behaving similiarly to the fully ordered samples[6].

3 EXPERIMENTAL PROCEDURE

Cold work and quenching from elevated temperatures have been shown to increase the ordering kinetics of many alloy systems. In this study, the influence of prior cold work and quenching on the hardening behaviour and ordering transformation in Pt 14 at. % Cu has been investigated.

Pt 14 at. % Cu undergoes an ordering transformation to form the $CuPt_7$ superlattice. It is expected that at the stoichiometric composition ($CuPt_7$, Pt 12.5 at. % Cu), the structure will become completely ordered upon heat treatment at temperatures that allow ordering, whereas the off-stoichiometric Pt 14 at. % Cu alloy will show a two-phase order-disorder equilibrium structure. For this reason, this study also makes a comparison of the hardening behaviour and ordering transformation of initially cold worked Pt 14 at. % Cu and initially cold worked Pt 12.5 at. % Cu after heat treatment.

The ordering transformation was investigated by using light microscopy, transmission electron microscopy (TEM) and x-ray diffraction (XRD). This section gives details of specimen preparation and the techniques used in this investigation.

3.1 SPECIMEN PREPARATION FOR HEAT TREATMENT EXPERIMENTS

Alloys of composition Pt 14 at.% Cu and Pt 12.5 at.% Cu were received in the cast state, in the form of buttons weighing about 10 g with thickness of about 5mm. The buttons were then cold rolled in a Dinkel laboratory rolling mill to reduce the thickness to 2.5 mm on average. The samples were then homogenised at 1000°C for 12 hours in an inert atmosphere. Subsequently these were checked for compositional homogeneity using energy dispersive spectroscopy (EDS). The homogenised buttons were then rolled to 90 per cent reduction from 2.5 mm, resulting in a final thickness of 250 μm.

3.2 HEAT TREATMENT EXPERIMENTS

All heat treatments were carried out in a vertical vacuum furnace using argon gas to create an inert atmosphere. Quenched samples were prepared by heat treatment at 1200°C for 2 hours, followed by quenching into water. Initially cold worked (90 per cent deformation) and initially quenched specimens were then heat treated at temperatures between 100°C and 700°C for 3 hours followed by furnace cooling to room temperature.

3.3 SPECIMEN PREPARATION FOR MICROHARDNESS MEASUREMENTS

Specimens were mounted using a conventional hot mounting technique. Specimens were ground on 1200 to 4000 grit grinding paper and then polished using 3 μm and 1 μm polishing paste to obtain a mirror finish. The hardness tests were done using a Zwick microhardness tester. A standard Vickers diamond indentor was used with a load of 100 gf.

3.4 SPECIMEN PREPARATION FOR LIGHT MICROSCOPY

The light microscopy specimens were ground and polished the same way as the microhardness specimens. Light micrographs of microstructures were obtained by etching samples with an electrolytic etchant as listed below:

- 25 ml HCl
- 25 g NaCl
- 65 ml distilled water

The etchant was heated until the salt was dissolved and a clear solution was obtained. Small amounts of water were added if salt was still suspended in solution. An alternating current was used at a potential of 10 V for a time period of 50 to 60 seconds using a graphite electrode.

3.5 SPECIMEN PREPARATION FOR TRANSMISSION ELECTRON MICROSCOPY

Specimens for TEM were punched into 3 mm diameter discs from bulk material of 250 μm thickness. Discs were then thinned to 100 μm by grinding on 1200 grit paper followed by heat treatments in the vertical vacuum furnace. After heat treatments, discs were mounted followed by polishing one side on a Gatan dimpler using 6 μm, 3 μm and 1 μm diamond paste with distilled water. The other side of the discs was then mechanically dimpled on a Gatan dimpler with a dimple depth set to 70 μm to achieve a thin area of 30 μm thickness. Final thinning of the specimens was done by milling in a Gatan Precision Ion Polishing System (PIPS). An accelerating voltage of 5 kV was used and the ion beam angle was set to 6° for the first hour of milling then to 4° to achieve an area that is electron transparent. Specimens were viewed in a JEOL

200CX transmission electron microscope. The operating parameters were 200kV and 82 cm camera length.

3.6 SPECIMEN PREPARATION FOR X-RAY DIFFRACTION

Specimens that were used for light microscopy and microhardness testing were repolished on 4000 grit paper followed by polishing on 3 μm and 1 μm diamond paste cloths. The XRD was carried out using a D8 Advance powder diffractometer. The specimens were scanned from 2θ angles of 30° to 143°, at 0.01° increments with three seconds as capture time.

4 RESULTS

This chapter presents results obtained from microhardness testing, light microscopy, x-ray diffraction and transmission electron microscopy, as well as simulation of the ordered structure.

4.1 MICROHARDNESS MEASUREMENTS

This section gives a detailed account of the microhardness measurements before and after heat treatment of initially cold worked Pt 14 at. % Cu, initially quenched Pt 14 at. % Cu and initially cold worked Pt 12.5 at. % Cu.

4.1.1 ISOCHRONAL HEAT TREATMENT OF PT 14 AT. % CU

After heat treatment of initially cold worked specimens at 100°C, 200°C , 300°C and 400°C the microhardness increased relative to the cold worked value of 241 HV, as shown in Figure 4-1. Heat treatment above 500°C resulted in a decrease in hardness relative to the initially cold worked value. After heat treatment of initially quenched specimens at 100°C, 200°C, 300°C and 400°C the microhardness increased slightly relative to the initially quenched value of 124 HV. The microhardness of initially quenched specimens after heat treatment at 500°C and 600°C remained the same as before heat treatment. Heat treatment at 700°C decreased the microhardness relative to the initial quenched value.

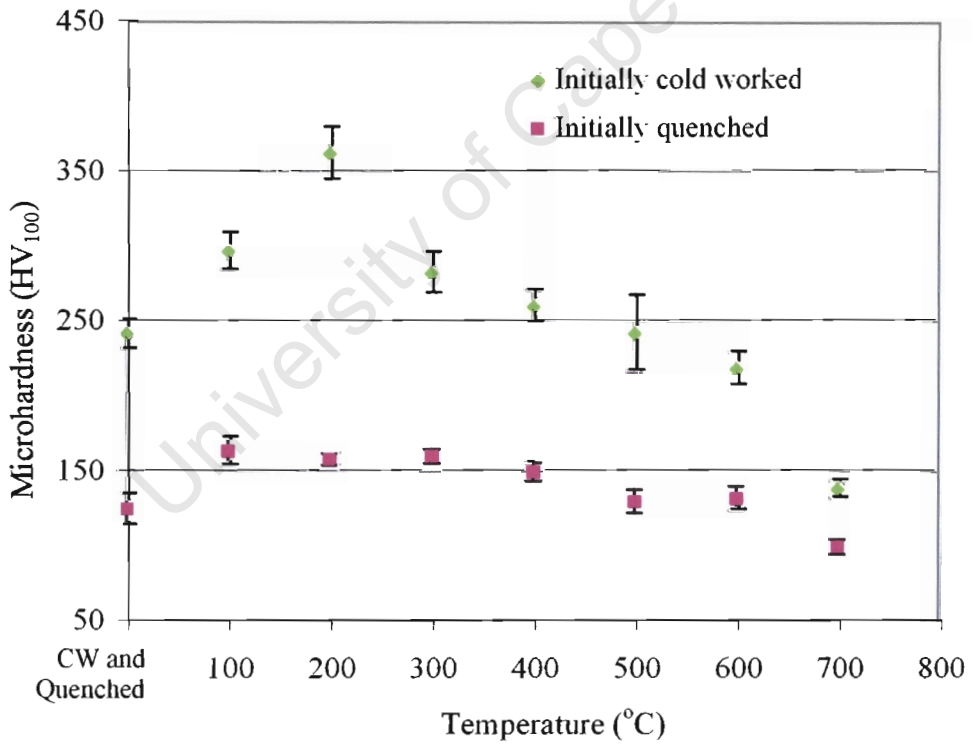

Figure 4-1 Graph of microhardness vs heat treatment temperature for initially cold worked and initially quenched Pt 14 at. % Cu after heat treatment for 3 hours.

4.1.2 ISOTHERMAL HEAT TREATMENT OF INITIALLY COLD WORKED PT 14 AT. % CU

Initially cold worked specimens exhibited the highest hardness after heat treatment at 200°C as shown in Figure 4-1. Prolonged heat treatment of initially cold worked specimens was carried out at 200°C to see if there is any significant change in hardness with time. Figure 4-2 shows that the hardness of initially cold worked specimens increased after heat treatment at 200°C for 30 minutes, but no further significant increase occured up to 720 hours.

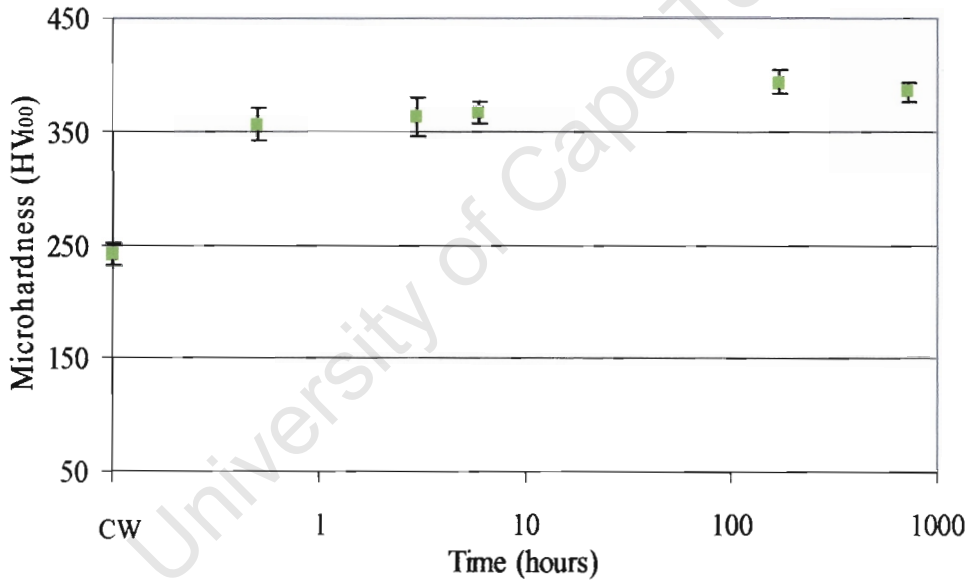

Figure 4-2 Graph of microhardness vs heat treatment time for initially cold worked Pt 14 at. % Cu after heat treatment at 200°C.

4.1.3 ISOTHERMAL HEAT TREATMENT OF INITIALLY QUENCHED PT 14 AT.% CU

Initially quenched specimens exhibited increased hardness after heat treatment at 100°C, 200°C, 300°C and 400°C. Prolonged heat treatment of initially quenched specimens was carried out at 300°C to see if there was any significant change in hardness with time. Figure 4-3 shows that the hardness of initially quenched specimens increased slightly after heat treatment up to 720 hours.

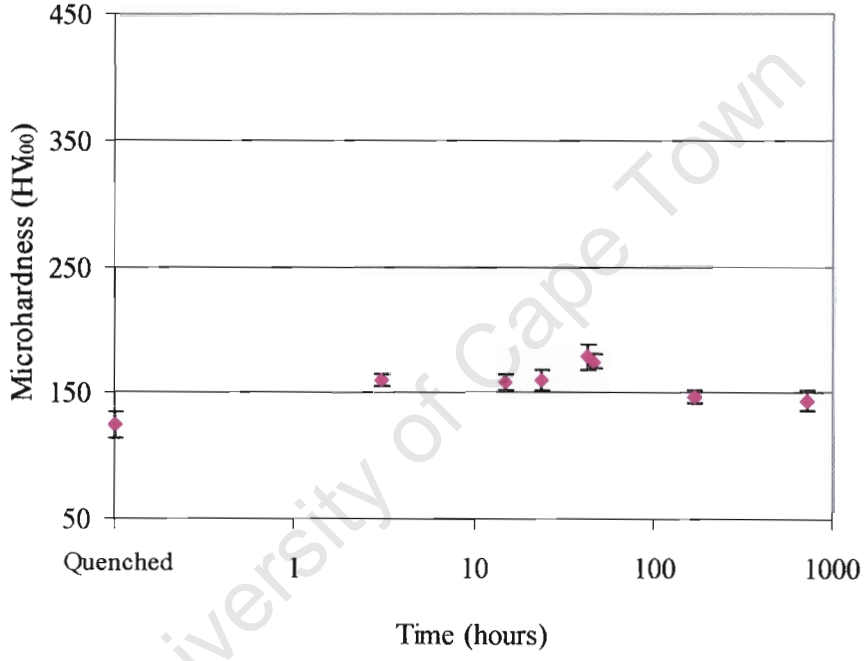

Figure 4-3 Graph of microhardness vs heat treatment time for initially quenched Pt 14 at. % Cu after heat treatment at 300°C.

4.1.4 ISOCHRONAL AND ISOTHERMAL HEAT TREATMENT OF PT 12.5 AT. % CU

Heat treatment of initially cold worked Pt 12.5 at. % Cu specimens resulted in a hardness increase for heat treatment temperatures below 400°C as shown in Figure 4-4. A hardness maximum of 372 HV was reached after heat treatment at 200°C, from the initially cold worked value of 289 HV. Heat treatment at 400°C and above led to a small decrease relative to the initial cold worked value.

Prolonged heat treatment was carried out at 200°C, the heat treatment temperature that resulted in maximum hardness, to monitor any significant change in hardness with time. Figure 4-5 shows that a measured hardness of about 360 HV was retained even after heat treatment for 720 hours.

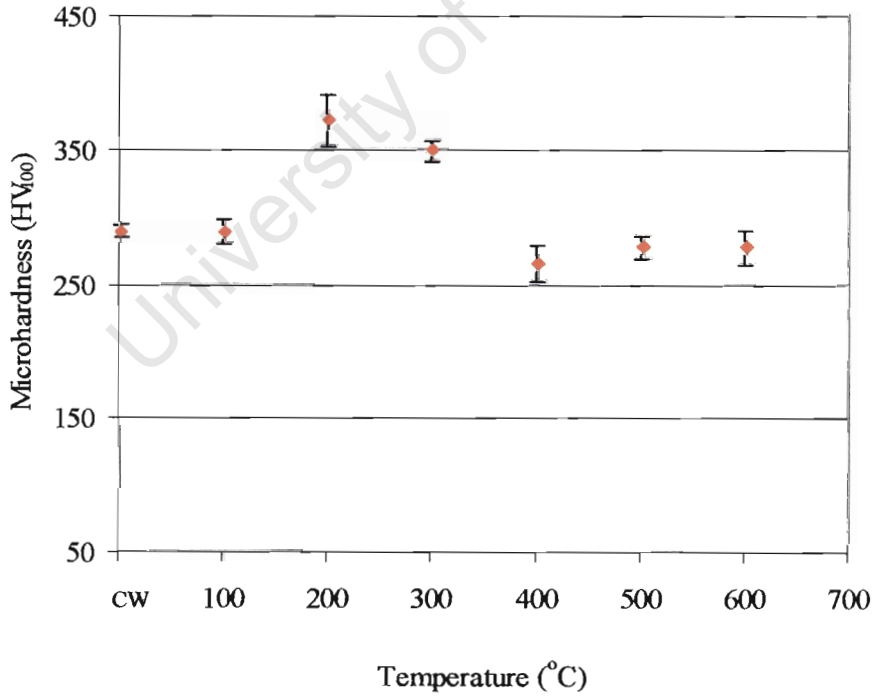

Figure 4-4 Graph of microhardness vs heat treatment temperature for initially cold worked Pt 12.5 at. % Cu after heat treatment for 3 hours.

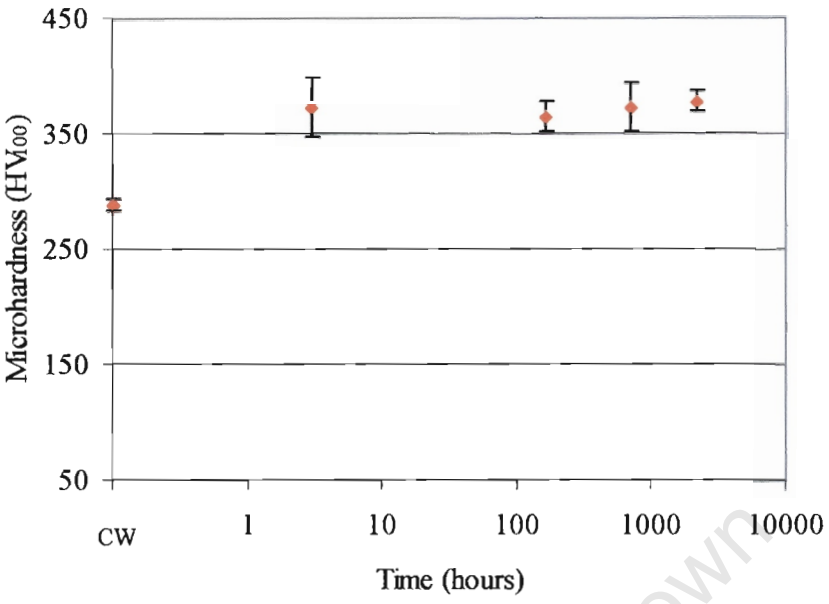

Figure 4-5 Graph of microhardness vs annealing time for initially cold worked Pt 12.5 at. % Cu after heat treatment at 200°C.

4.2 LIGHT MICROSCOPY

Light microscopy was carried out to determine if there is a change in microstructure after the heat treatment of initially cold worked and initially quenched Pt 14 at. % Cu specimens.

The microstructure of a cold worked specimen is shown in Figure 4-6. The specimen shows a heavily deformed structure with elongated grains. After heat treatment of initially cold worked Pt 14 at. % Cu at 200°C for 3 hours, the microstructure remained heavily deformed and there were no visible changes that would indicate the cause of hardening, as shown in Figure 4-7. Deformed microstructures were still observed after heat treatment at 500°C and 600°C as shown in Figure 4-8 and Figure 4-9 respectively. Initially cold worked Pt 14 at. % Cu showed a recrystallised microstructure after heat treatment at 700°C for 3 hours as shown in Figure 4-10.

Isothermal heat treatment of initially cold worked Pt 14 at. % Cu specimens at 200°C for 1 week and 2 weeks resulted in the microstructures showed in Figure 4-11 and Figure 4-12 respectively. Microstructures remained heavily deformed and there were no visible changes.

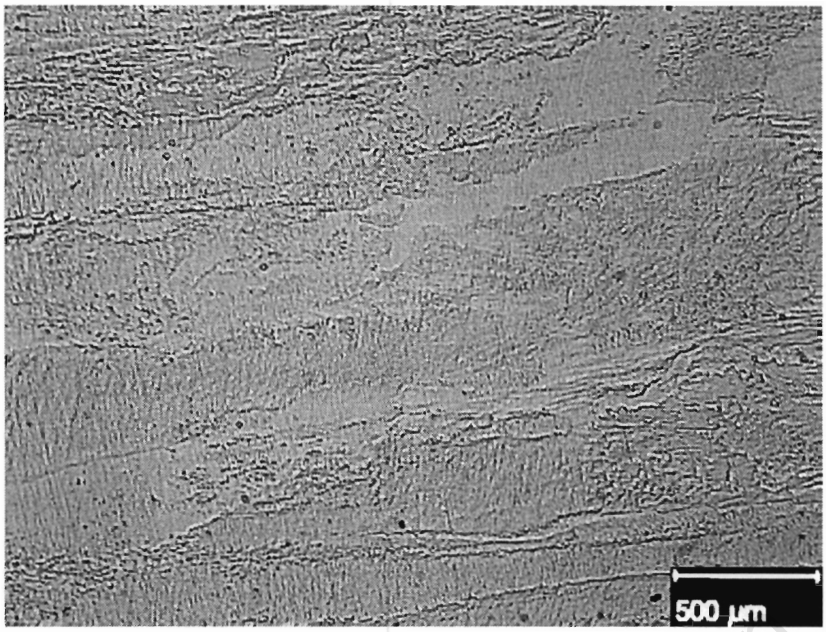

Figure 4-6 Light micrograph of Pt 14 at. % Cu in the cold-worked condition, showing a deformed microstructure.

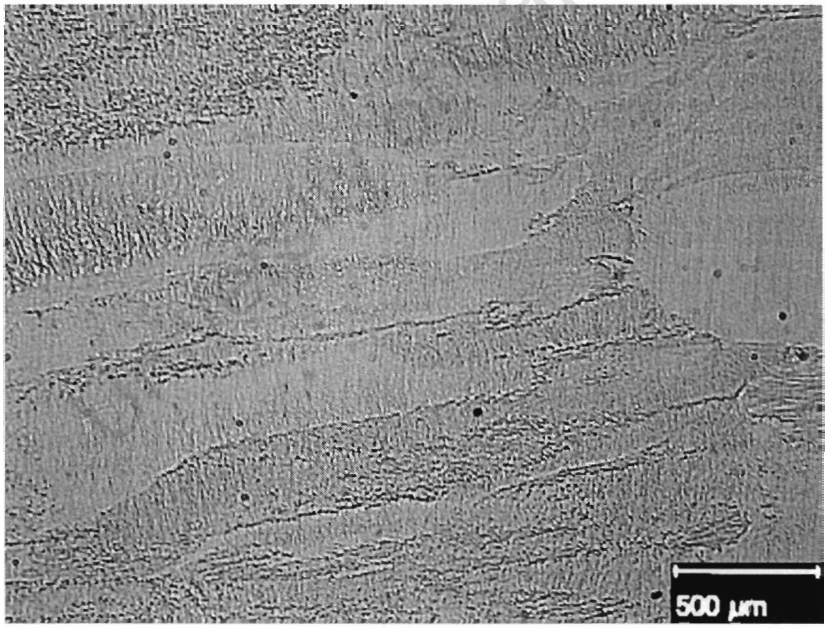

Figure 4-7 Light micrograph of initially cold worked Pt 14 at. % Cu after heat treatment at 200°C for 3 hours, showing a deformed microstructure.

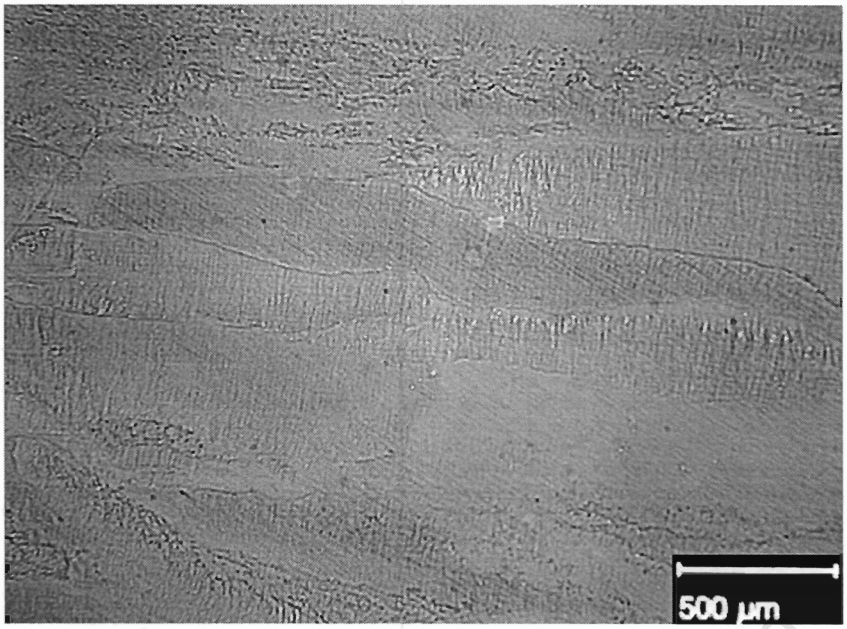

Figure 4-8 Light micrograph of initially cold worked Pt 14 at. % Cu after heat treatment at 500°C for 3 hours, showing a deformed microstructure.

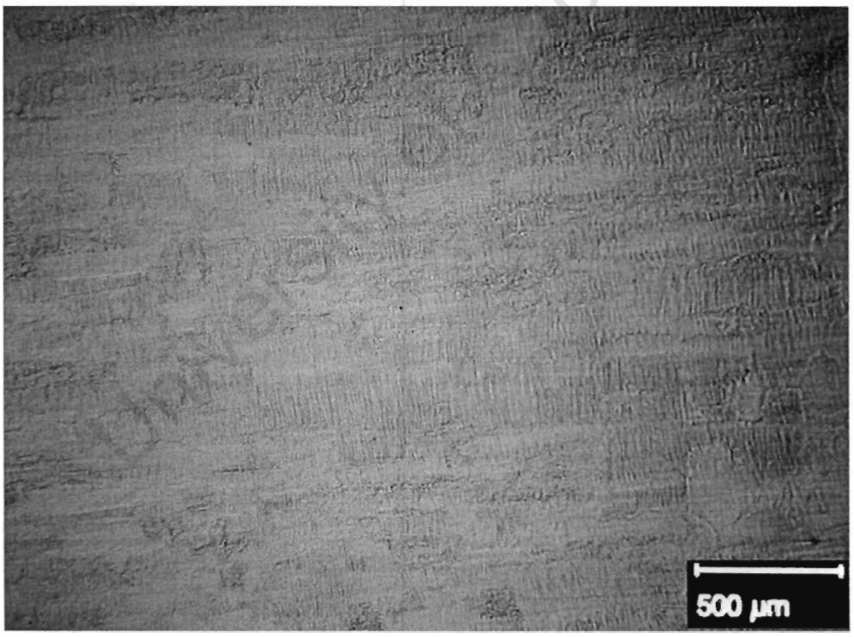

Figure 4-9 Light micrograph of initially cold worked Pt 14 at. % Cu after heat treatment at 600°C for 3 hours, showing a deformed microstructure.

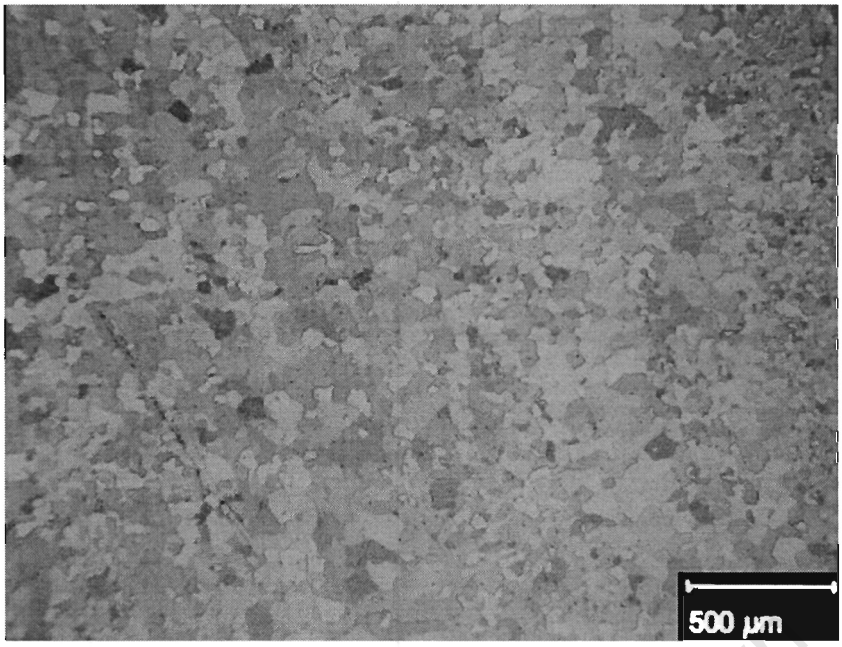

Figure 4-10 Light micrograph of initially cold worked Pt 14 at. % Cu after heat treatment at 700°C for 3 hours, showing a recrystallised microstructure.

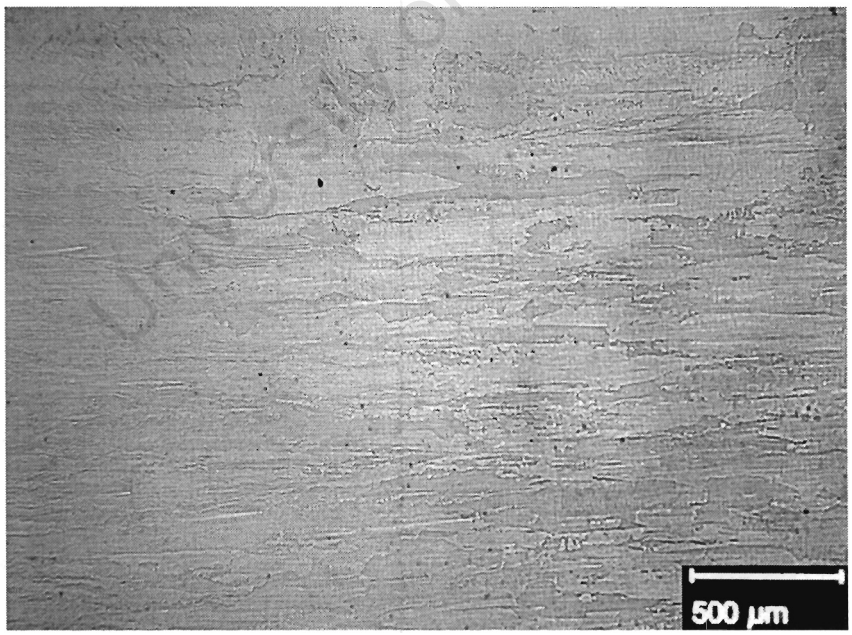

Figure 4-11 Light micrograph of initially cold worked Pt 14 at. % Cu after heat treatment at 200°C for 1 week, showing a deformed microstructure.

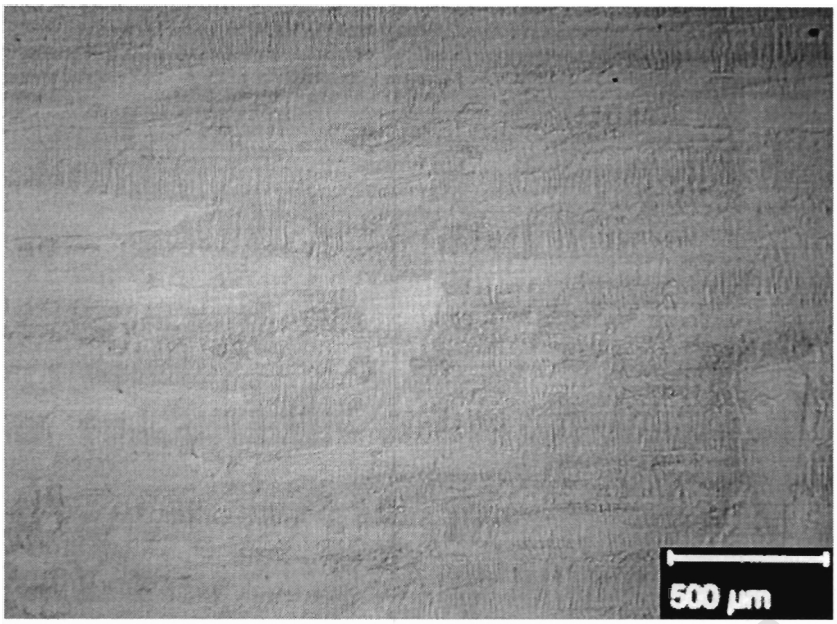

Figure 4-12 Light micrograph of initially cold worked Pt 14 at. % Cu after heat treatment at 200°C for 2 weeks, showing a deformed microstructure.

A light micrograph of quenched Pt 14 at. % Cu is shown in Figure 4-13. After heat treating the initially quenched specimen at 300°C for 3 hours, there was no change in microstructure that could account for the hardening occurring at this temperature, as seen in Figure 4-14. Light micrographs of initially quenched specimens after heat treatment at 500°C and 700°C are shown in Figure 4-15 and Figure 4-16 respectively. No change in the microstructure was observed after heat treatment at 500°C and 600°C, whereas after heat treatment at 700°C grain growth is observed.

Heat treatment of initially quenched specimens at 300°C for 1 week and 1 month resulted in no major changes in the microstructures that could account for the hardening, as shown in Figure 4-17 and Figure 4-18 respectively.

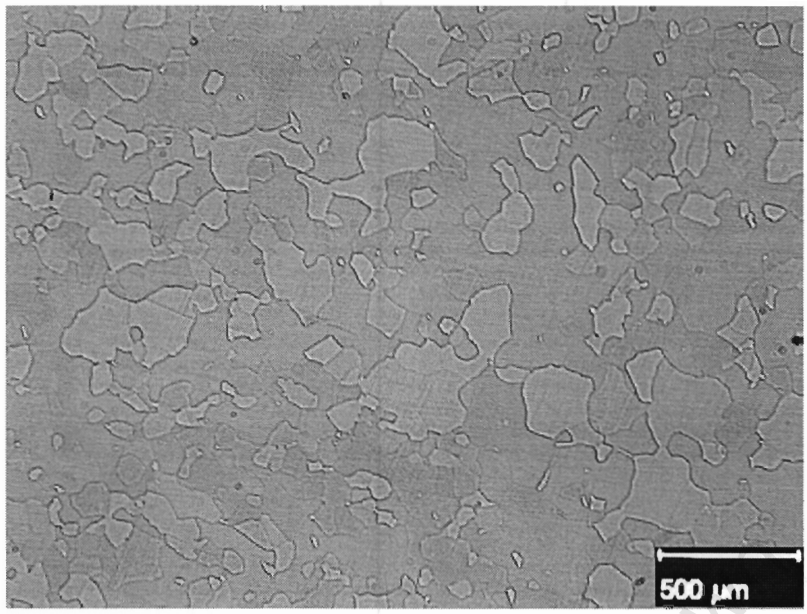

Figure 4-13 Light micrograph of quenched Pt 14 at. % Cu, showing an equiaxed grain structure.

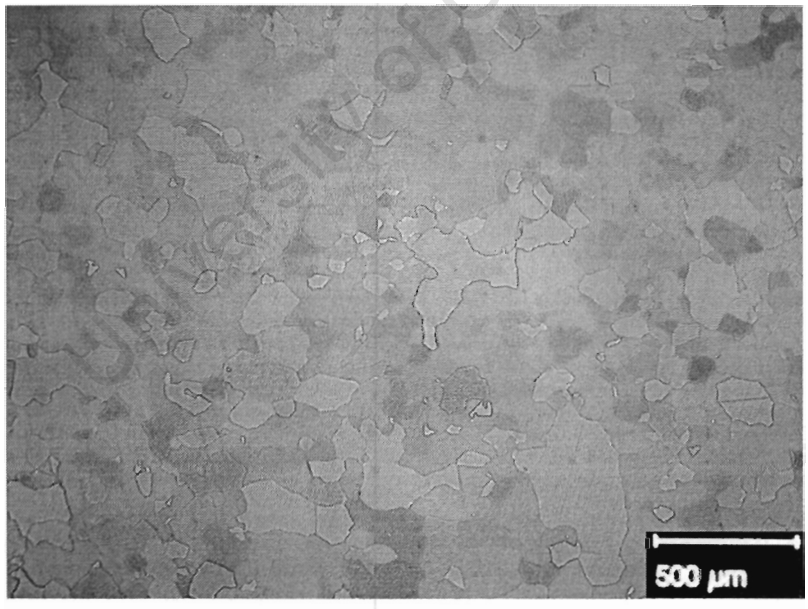

Figure 4-14 Light micrograph of initially quenched Pt 14 at. % Cu after heat treatment at 300°C for 3 hours showing an unchanged grain structure.

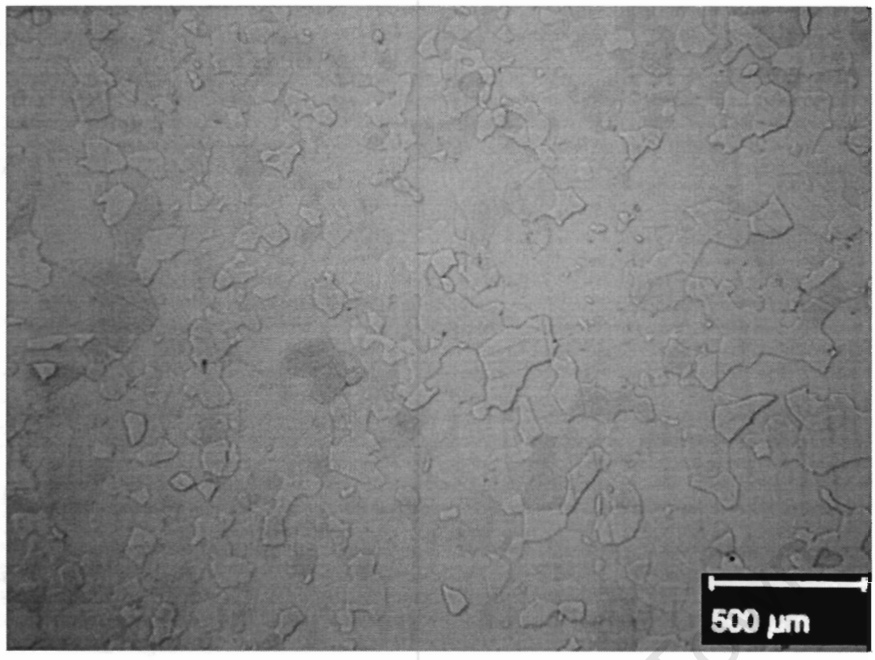

Figure 4-15 Light micrograph of initially quenched Pt 14 at. % Cu after heat treatment at 500°C for 3 hours showing an unchanged grain structure.

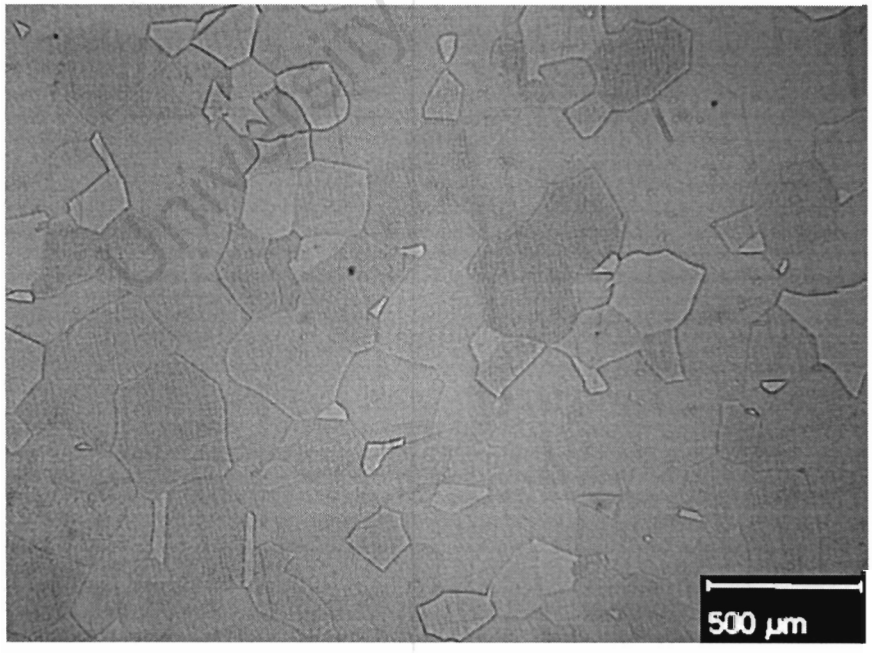

Figure 4-16 Light micrograph of initially quenched Pt 14 at. % Cu after heat treatment at 700°C for 3 hours showing an increased grain size.

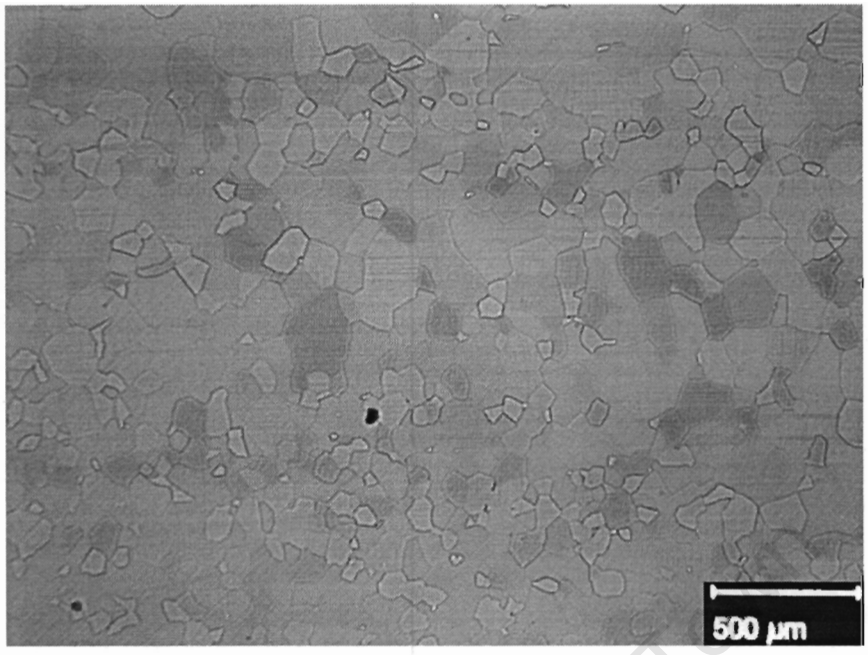

Figure 4-17 Light micrograph of initially quenched Pt 14 at. % Cu after heat treatment at 300°C for 1 week showing an unchanged grain structure.

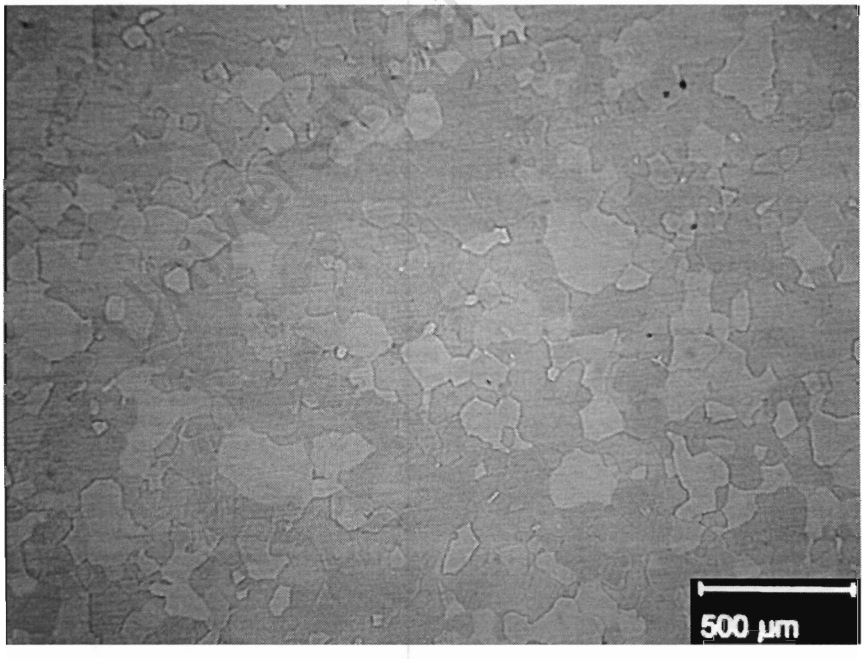

Figure 4-18 Light micrograph of initially quenched Pt 14 at. % Cu after heat treatment at 300°C for 1 month showing an unchanged grain structure.

4.3 X-RAY DIFFRACTION

This section gives the x-ray diffraction spectra of initially cold worked and initially quenched specimens before and after heat treatment at temperatures that resulted in optimum hardness.

Cold worked specimens displayed the x-ray diffraction spectrum as shown in Figure 4-19, which shows the peaks associated with a fundamental fcc crystal structure.

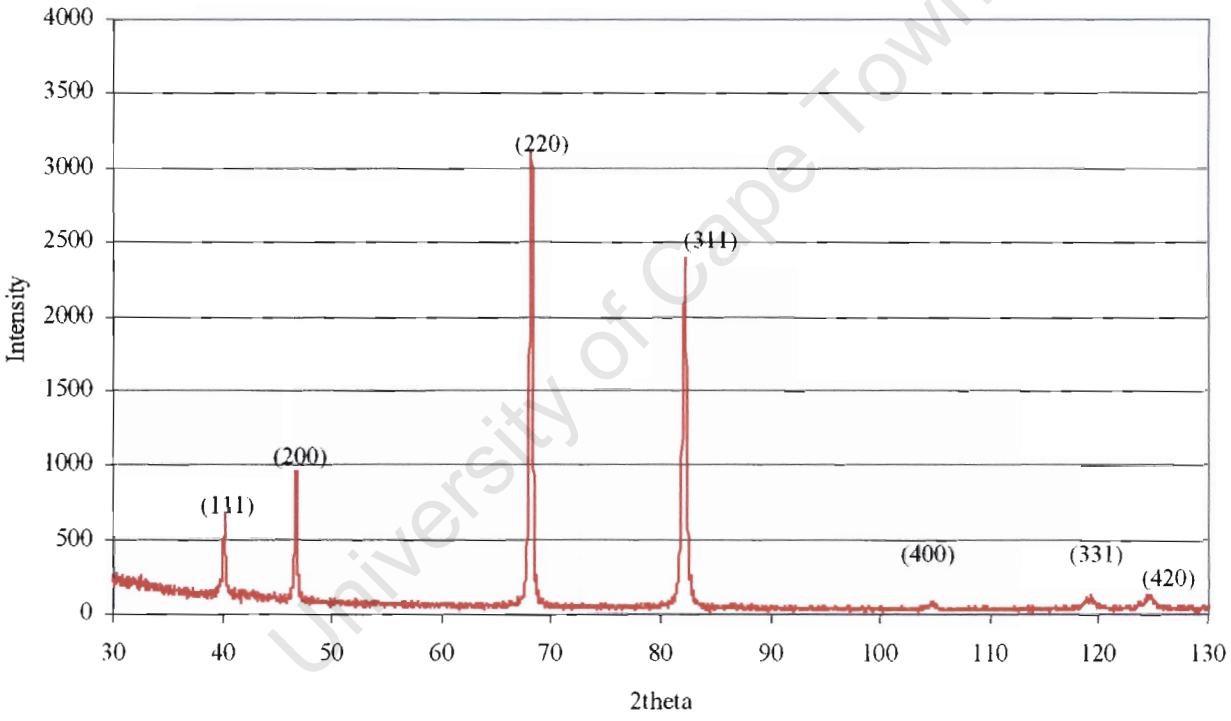

Figure 4-19 X-ray diffraction spectrum of Pt 14 at. % Cu in the cold worked condition.

After heat treatment of the initially cold worked sample at 200°C for 48 hours the peak distribution and peak intensity are no different from the initially cold worked sample as shown in Figure 4-20.

The lattice parameter before and after heat treatment of cold worked Pt 14 at. % Cu was very similar, i.e. 3.789 Å and 3.782 Å respectively.

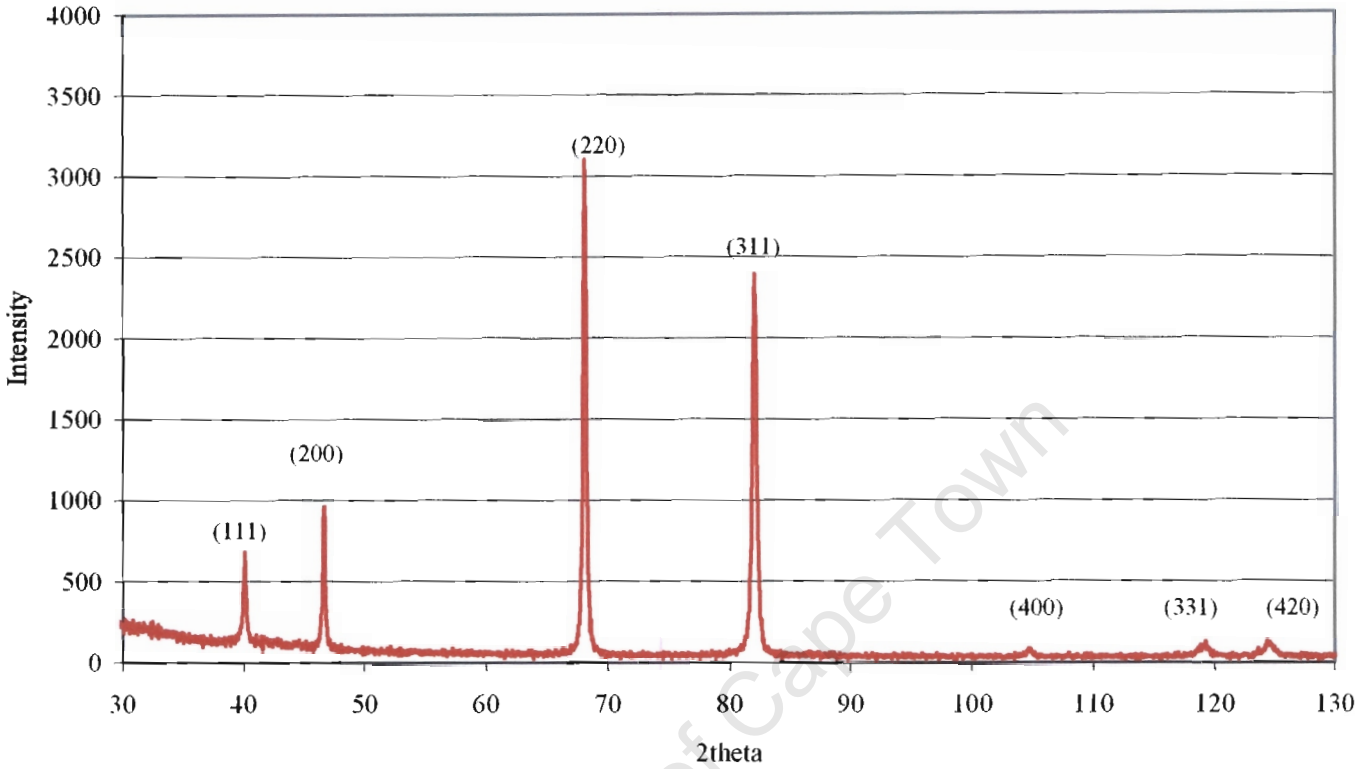

Figure 4-20 X-ray diffraction spectrum of initially cold worked Pt 14 at. % Cu after heat treatment at 200°C.

Initially quenched and heat treated specimens displayed the x-ray diffraction spectra illustrated in Figure 4-21 and Figure 4-22 respectively. The intensity of the 111, 200, 220 and 311 planes increased slightly after heat treatment at 300°C for 48 hours, however the positions of the peaks remain the same. An increased intensity can be associated with a change in the positions of atoms, but a change in atomic positions resulting in formation of a superlattice would also be expected to result in new peaks. The XRD spectra after heat treatment therefore do not show evidence of a significant change in atomic configuration as a result of heat treatment.

The lattice parameter before and after heat treatment of quenched Pt 14 at. % Cu was very similar, i.e. 3.775 Å and 3.782 Å respectively.

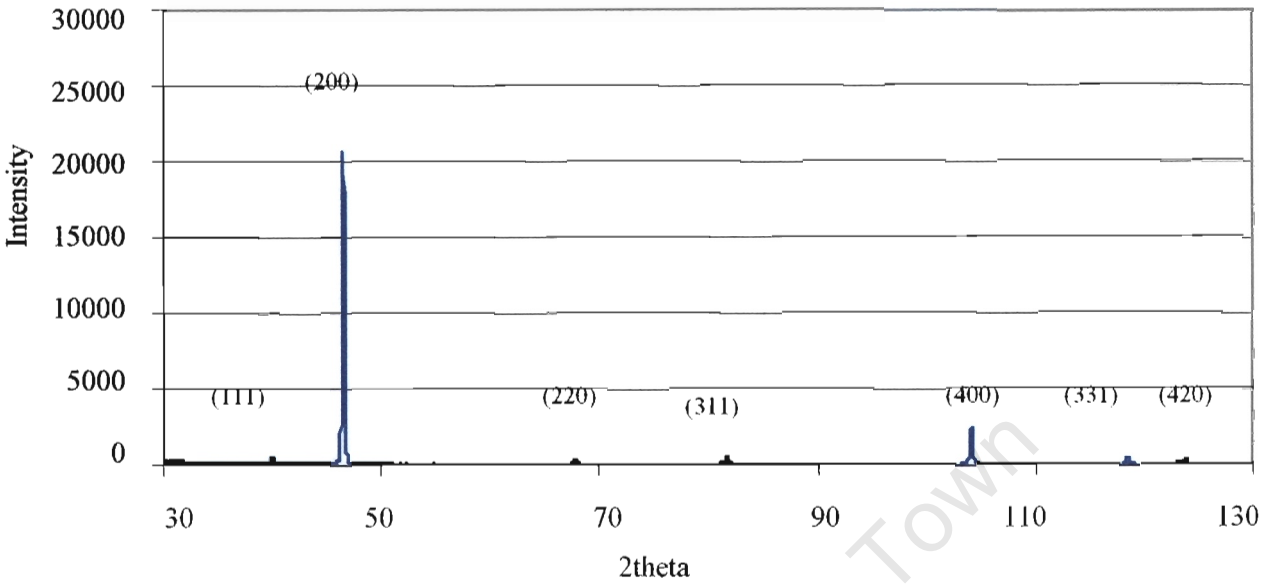

Figure 4-21 X-ray diffraction spectrum of quenched Pt 14 at. % Cu.

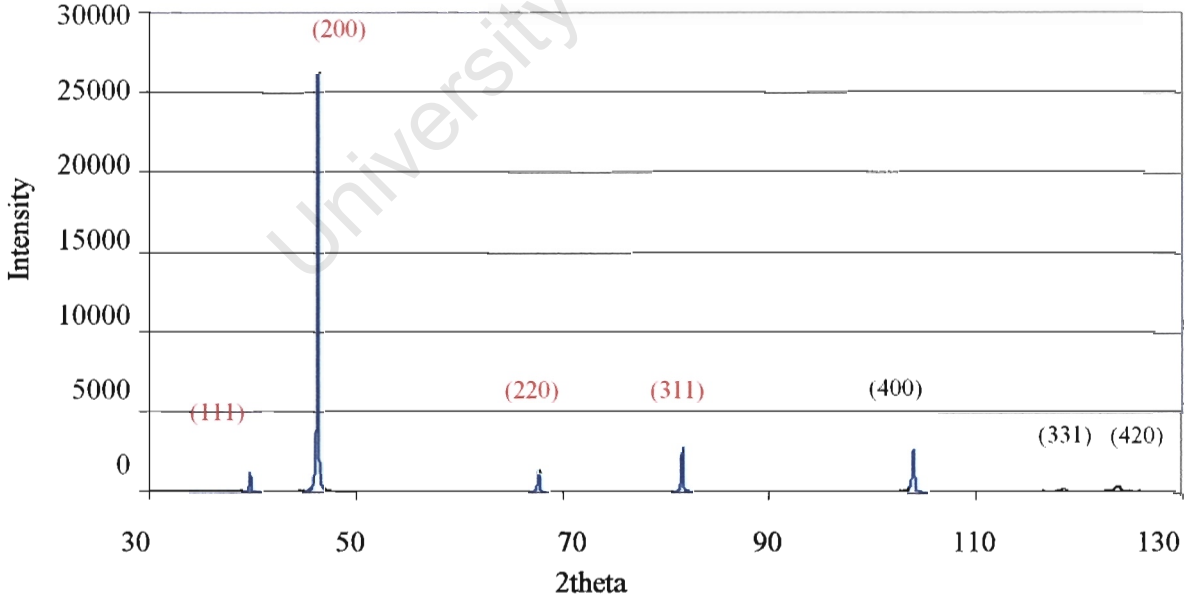

Figure 4-22 X-ray diffraction spectrum of initially quenched Pt 14 at. % Cu after heat treatment at 300°C.

4.4 TRANSMISSION ELECTRON MICROSCOPY

This section gives zone axis electron diffraction patterns from cold worked Pt 14 at. % Cu specimens, followed by initially cold worked and initially quenched Pt 14 at. % Cu after heat treatment. The section ends with electron patterns of initially cold worked Pt 12.5 at. % Cu after heat treatment at 200°C.

4.4.1 ELECTRON DIFFRACTION PATTERNS FROM COLD WORKED PT 14 AT. % CU SPECIMENS

The electron diffraction patterns in Figure 4-23 and Figure 4-24 are from the cold worked samples. They reveal only the fundamental reflections associated with a fcc crystal structure. The same structure was also observed for quenched samples.

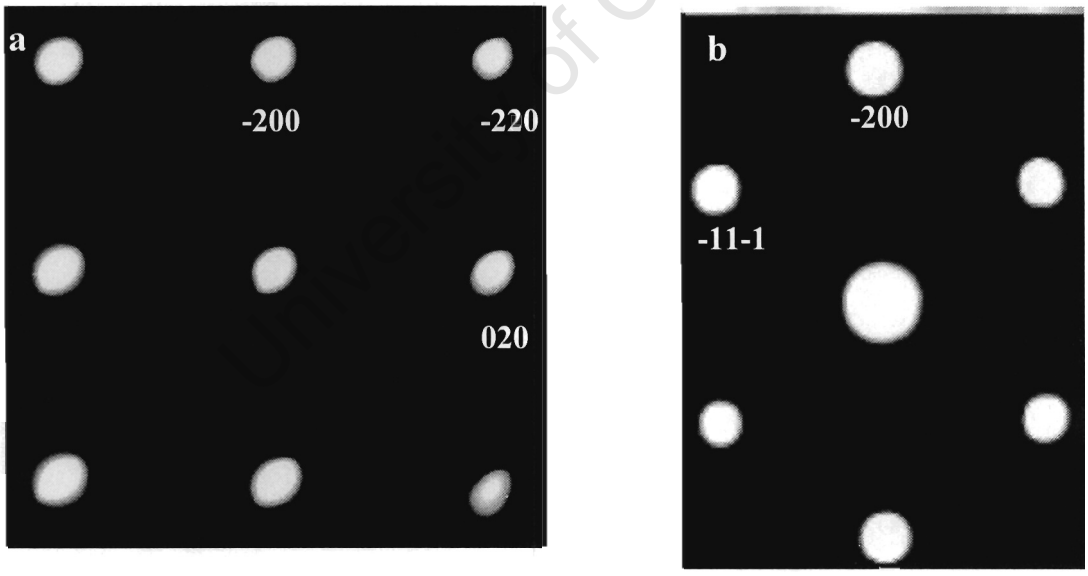

Figure 4-23 Electron diffraction patterns from cold worked Pt 14 at. % Cu viewed along the (a) $[001]_{fcc}$ and (b) $[011]_{fcc}$ zone axes.

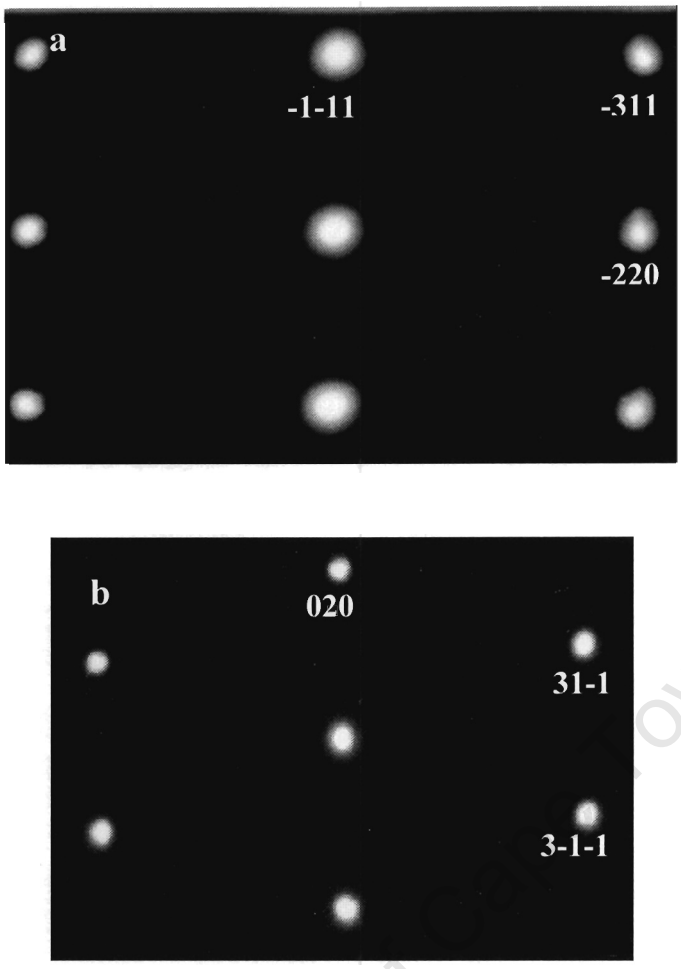

Figure 4-24 Electron diffraction patterns from cold worked Pt 14 at. % Cu viewed along the (a) $[112]_{fcc}$ and (b) $[103]_{fcc}$ zone axes.

4.4.2 ELECTRON DIFFRACTION PATTERNS OF INITIALLY COLD WORKED PT 14 AT. % CU SPECIMENS AFTER HEAT TREATMENT

This section shows electron diffraction patterns of cold worked Pt 14 at. % Cu after heat treatment. Specimens heat treated at 200°C, 400°C and 500°C were investigated.

Figure 4-25 shows a zone axis electron diffraction pattern of initially cold worked Pt 14 at. % Cu after heat treatment for 3 hours at 200°C. It is indexed as viewed along the $[001]_{fcc}$ axis and shows the main fcc lattice reflections indexed as (002), (020) and (022). In addition to these reflections, there are reflections at every one half position along the <002> and <022> type directions. Figure 4-26 and Figure 4-27 show electron diffraction patterns indexed as viewed along the $[112]_{fcc}$ and $[103]_{fcc}$ zone axes respectively. The $[112]_{fcc}$ electron diffraction pattern reveals the main fcc lattice reflections indexed as (111), (131) and (022). It also reveals superlattice reflections halfway along every fundamental fcc lattice direction. The $[103]_{fcc}$ electron diffraction pattern reveals the main fcc lattice reflections indexed as (020) and (131). It also reveals superlattice reflections halfway along every fundamental fcc lattice direction. Figure 4-28 shows electron diffraction pattern viewed along the $[011]_{fcc}$ zone axis. In addition to the main fcc reflections, superlattice reflections are visible at one half positions along the <111> and <200> type directions.

This superlattice was also observed after heat treatment at 400°C as shown in Figure 4-29. Heat treatment at 500°C did not result in the formation of this superlattice as seen in Figure 4-30.

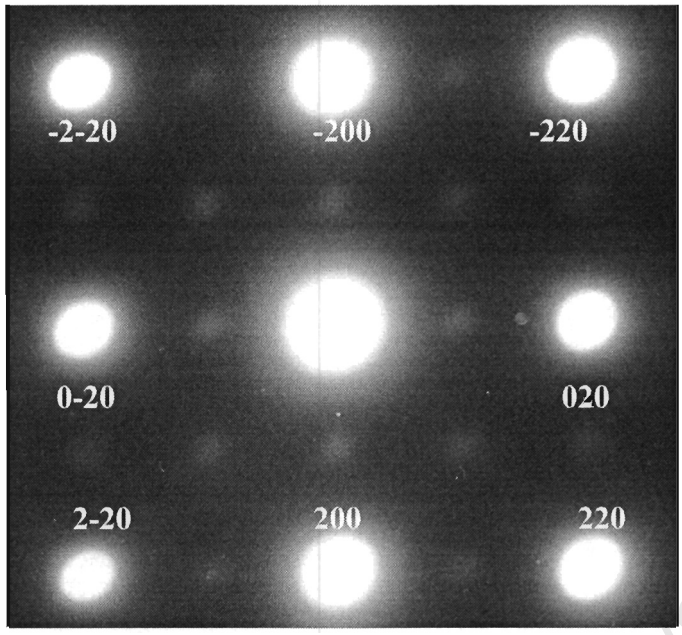

Figure 4-25 Electron diffraction pattern from initially cold worked Pt 14 at. % Cu after heat treatment at 200°C for 3 hours, viewed along the $[001]_{fcc}$ zone axis.

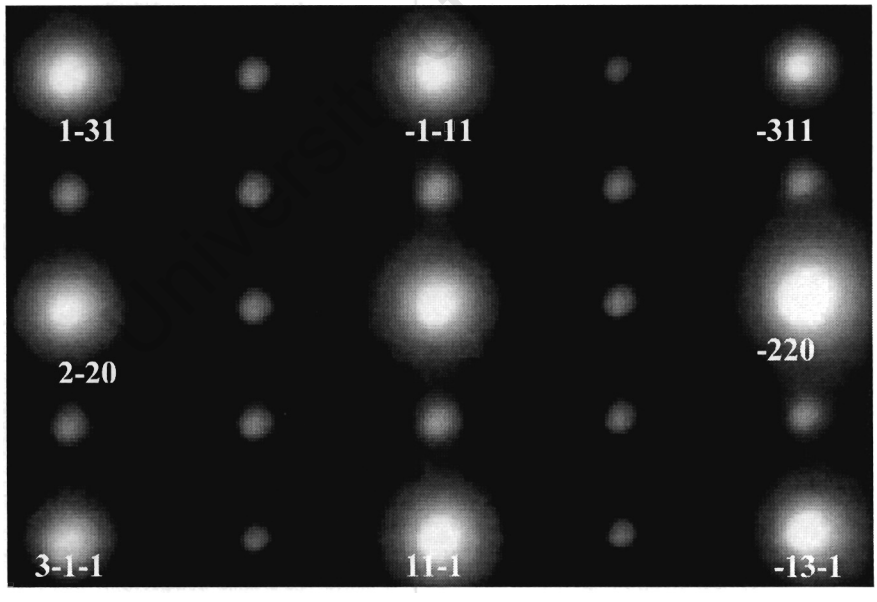

Figure 4-26 Electron diffraction pattern from initially cold worked Pt 14 at. % Cu after heat treatment at 200°C for 3 hours, viewed along the $[112]_{fcc}$ zone axis.

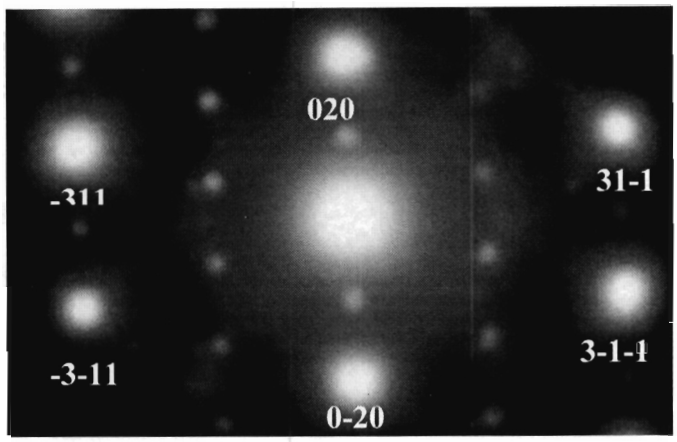

Figure 4-27 Electron diffraction patterns from initially cold worked Pt 14 at. % Cu after heat treatment at 200°C for 3 hours, viewed along the $[103]_{fcc}$ zone axis.

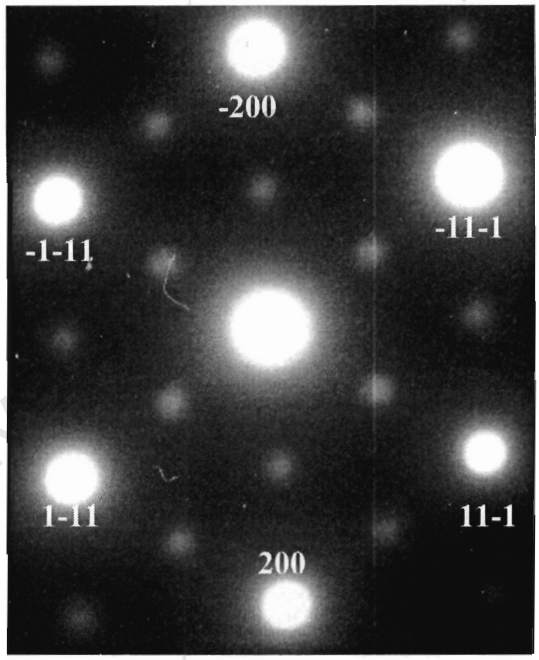

Figure 4-28 Electron diffraction patterns from initially cold worked Pt 14 at. % Cu after heat treatment at 200°C for 3 hours, viewed along the $[011]_{fcc}$ zone axis.

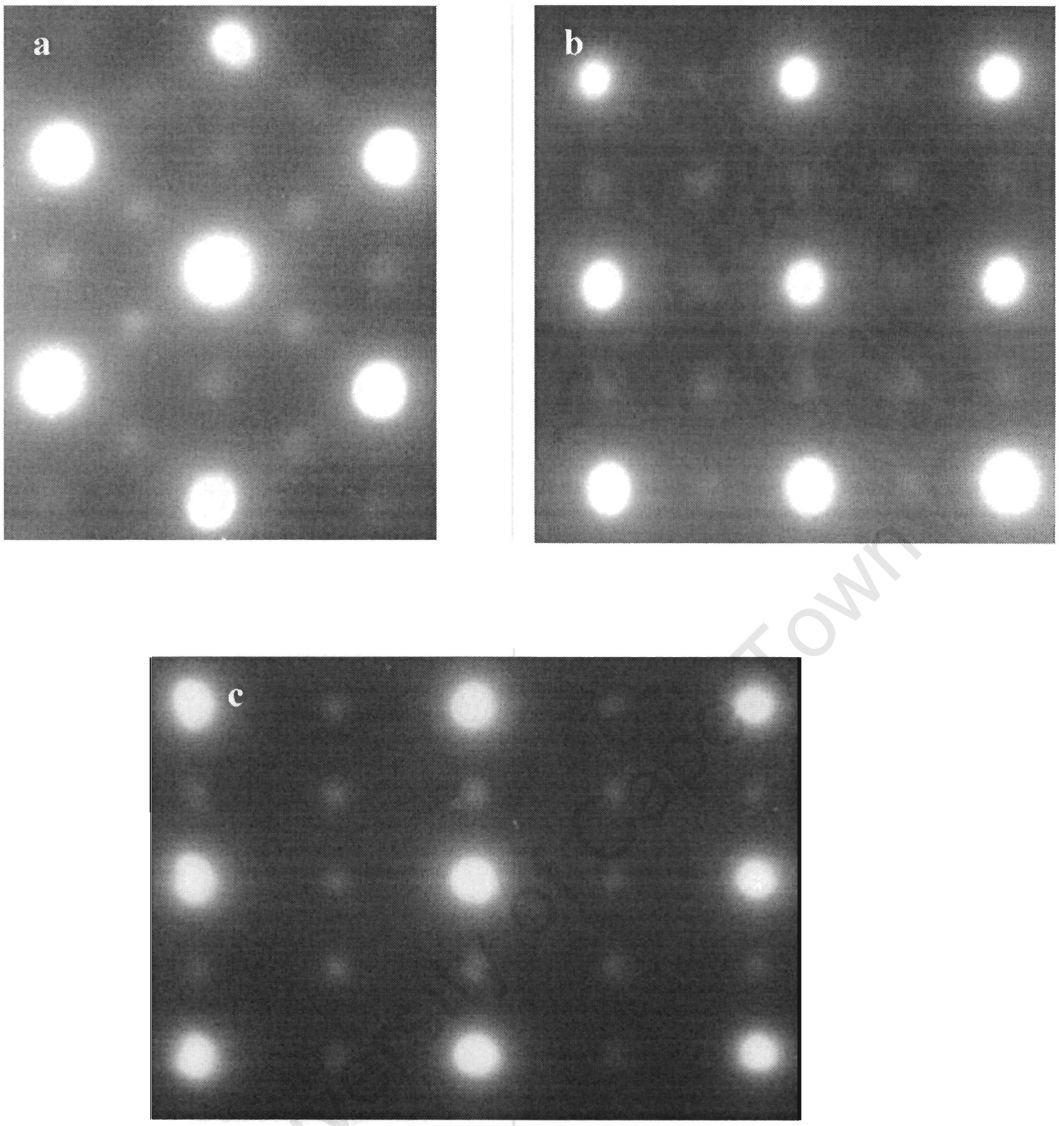

Figure 4-29 Electron diffraction patterns from initially cold worked Pt 14 at. % Cu after heat treatment at 400°C for 3 hours, viewed along the (a) $[011]_{fcc}$, (b) $[001]_{fcc}$, (c) $[112]_{fcc}$ zone axes.

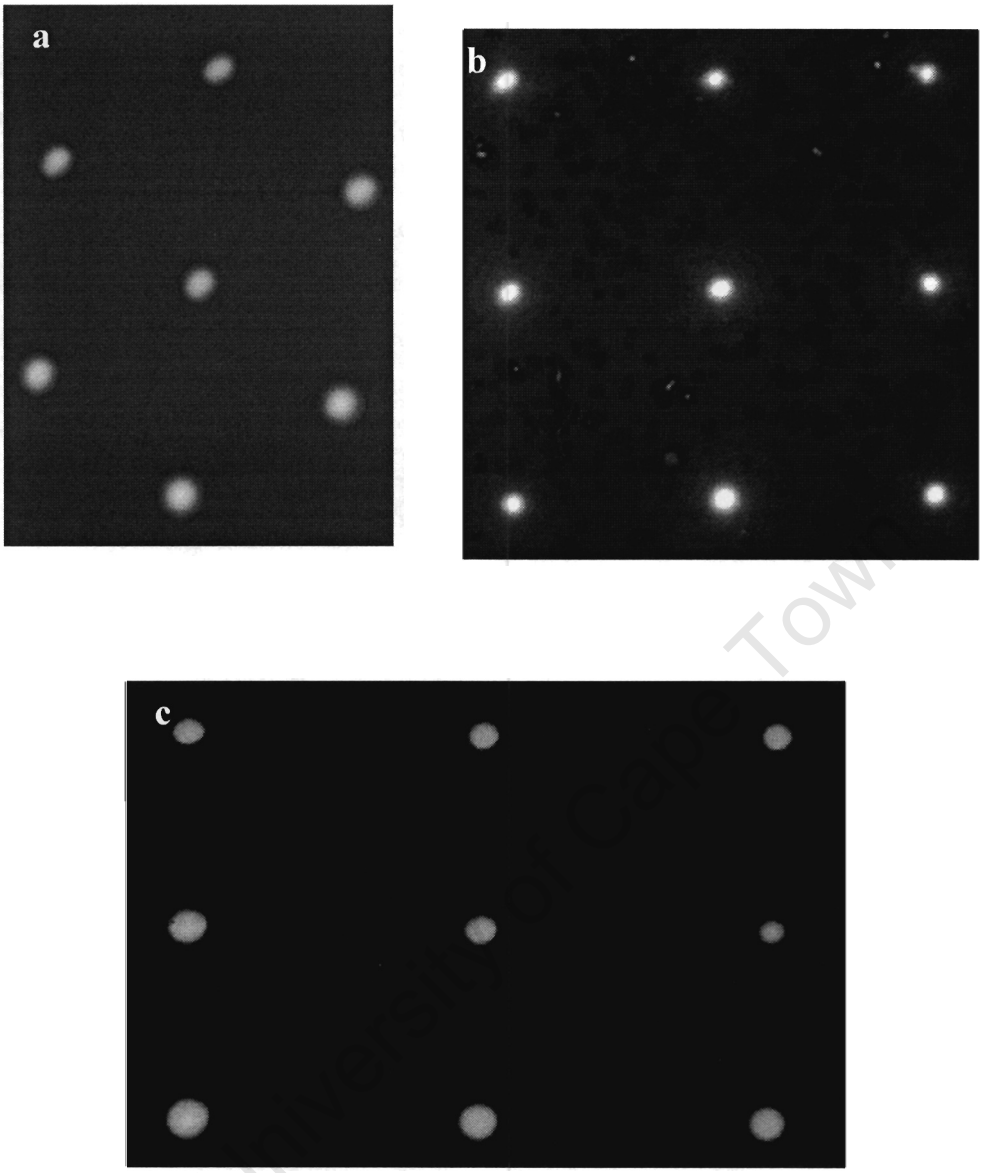

Figure 4-30 Electron diffraction patterns from initially cold worked Pt 14 at. % Cu after heat treatment at 500°C for 3 hours, viewed along the (a) $[011]_{fcc}$, (b) $[001]_{fcc}$, (c) $[112]_{fcc}$ zone axes.

4.4.3 ELECTRON DIFFRACTION PATTERNS OF INITIALLY QUENCHED PT 14 AT. % CU SPECIMENS AFTER HEAT TREATMENT

This section shows electron diffraction patterns of quenched Pt 14 at. % Cu after heat treatment. Specimens heat treated at 200°C, 300°C and 500°C were investigated. Figure 4-31 shows the electron diffraction patterns of initially quenched Pt 14 at. % Cu after heat treatment at 300°C for 3 hours. It shows electron diffraction patterns indexed as viewed along the $[001]_{fcc}$, $[112]_{fcc}$, $[103]_{fcc}$ and $[011]_{fcc}$ zone axes. The $[001]_{fcc}$ electron diffraction pattern shows the main fcc lattice reflections indexed as (002), (020) and (022). In addition to these reflections, there are reflections at every one half position along the <002> and <022> type directions. The $[112]_{fcc}$ electron diffraction pattern reveals the main fcc lattice reflections indexed as (111), (131) and (022). It also reveals superlattice reflections halfway along every fundamental fcc lattice direction. The $[103]_{fcc}$ electron diffraction pattern reveals the main fcc lattice reflections indexed as (020) and (131). It also reveals superlattice reflections halfway along every fundamental fcc lattice direction. In addition to the main fcc reflections, the $[011]_{fcc}$ electron diffraction pattern shows superlattice reflections at one half positions along the <111> and <200> type directions.

This superlattice was also observed after heat treatment at 200°C as shown in Figure 4-32. Heat treatment at 500°C did not result in the formation of this superlattice as seen in Figure 4-33.

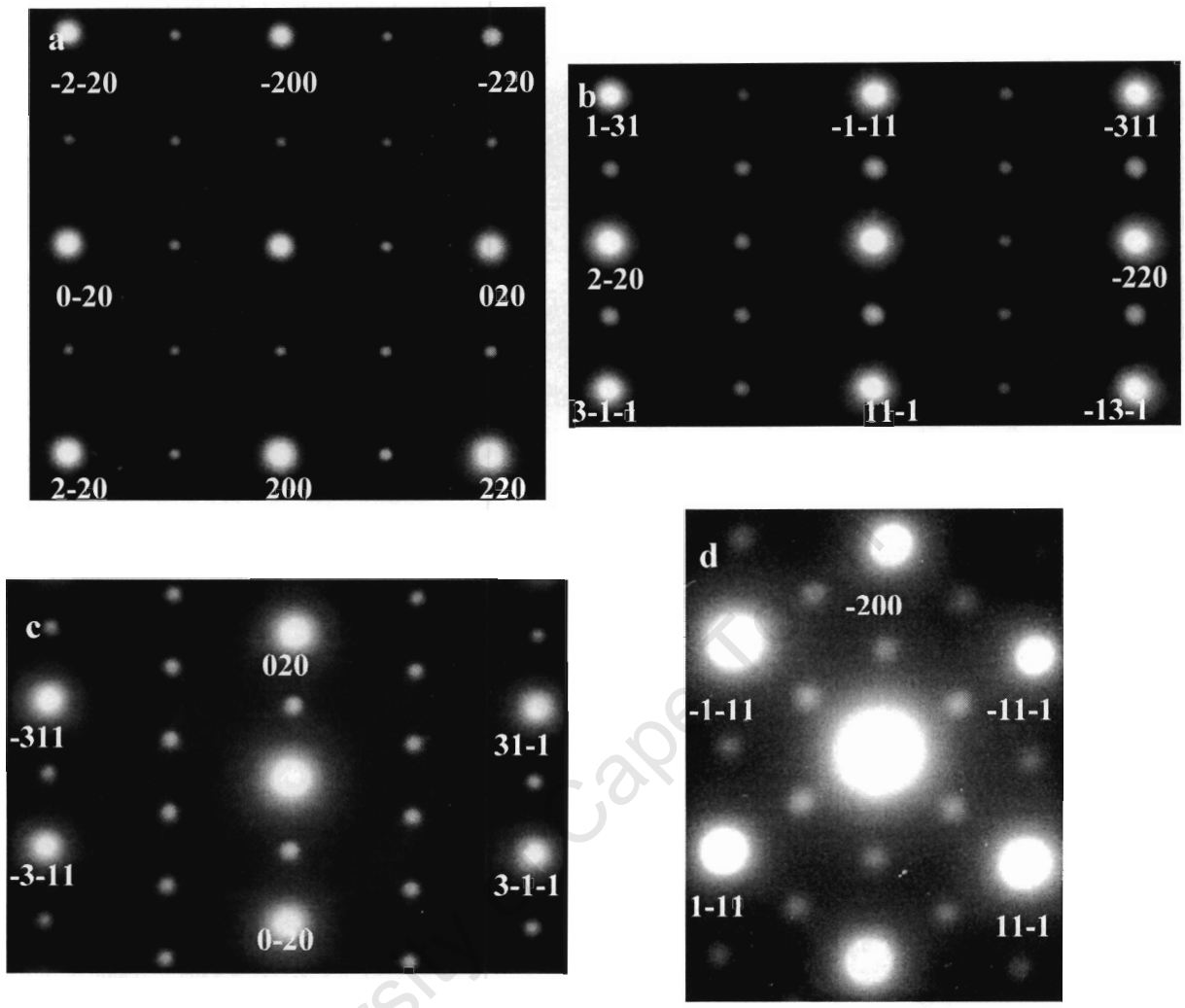

Figure 4-31 Electron diffraction patterns from initially quenched Pt 14 at. % Cu after heat treatment at 300°C for 3 hours, viewed along the (a) $[001]_{fcc}$, (b) $[112]_{fcc}$, (c) $[103]_{fcc}$ and (d) $[011]_{fcc}$ zone axes.

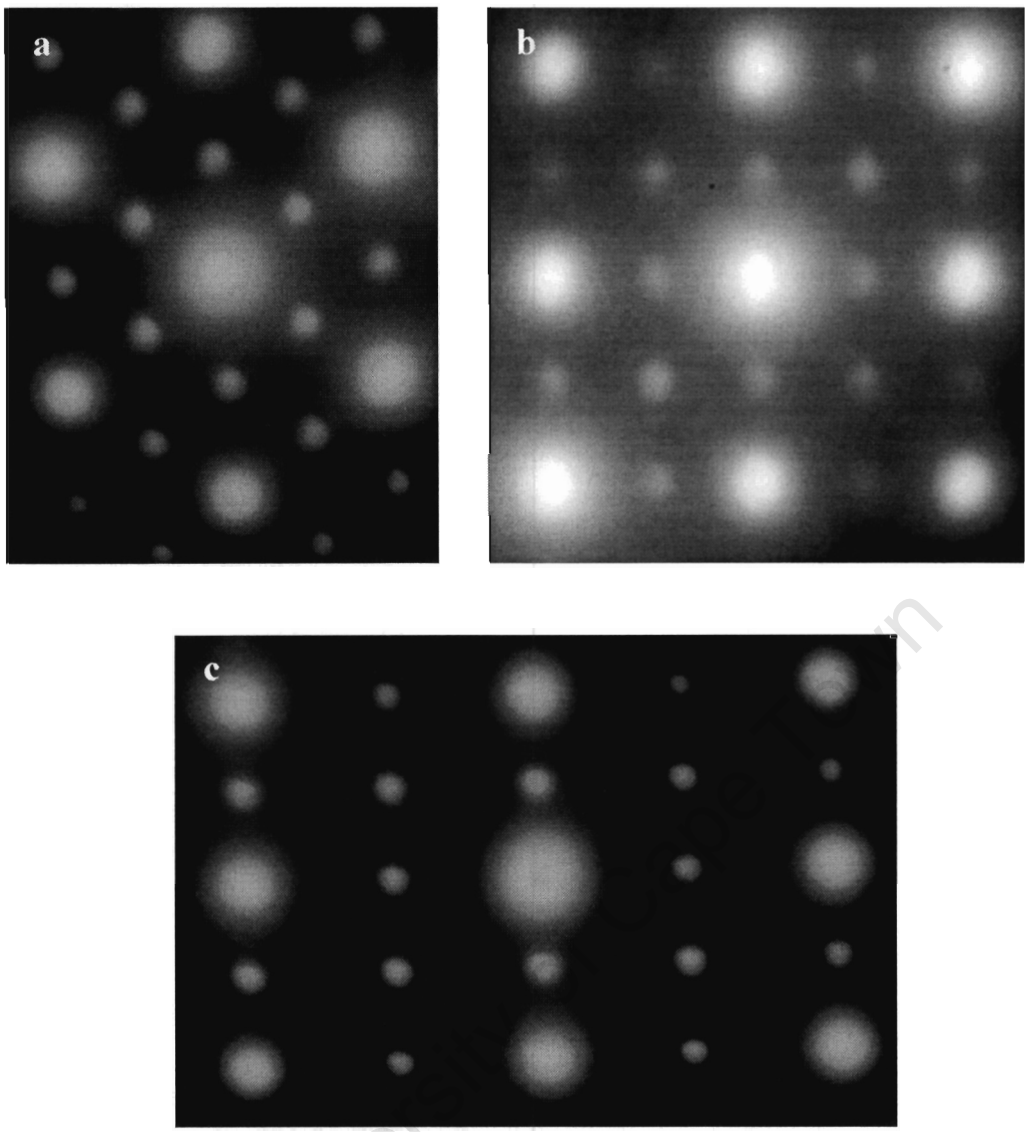

Figure 4-32 Electron diffraction patterns from initially quenched Pt 14 at. % Cu after heat treatment at 200°C for 3 hours, viewed along the (a) $[011]_{fcc}$, (b) $[001]_{fcc}$ and (c) $[112]_{fcc}$ zone axes.

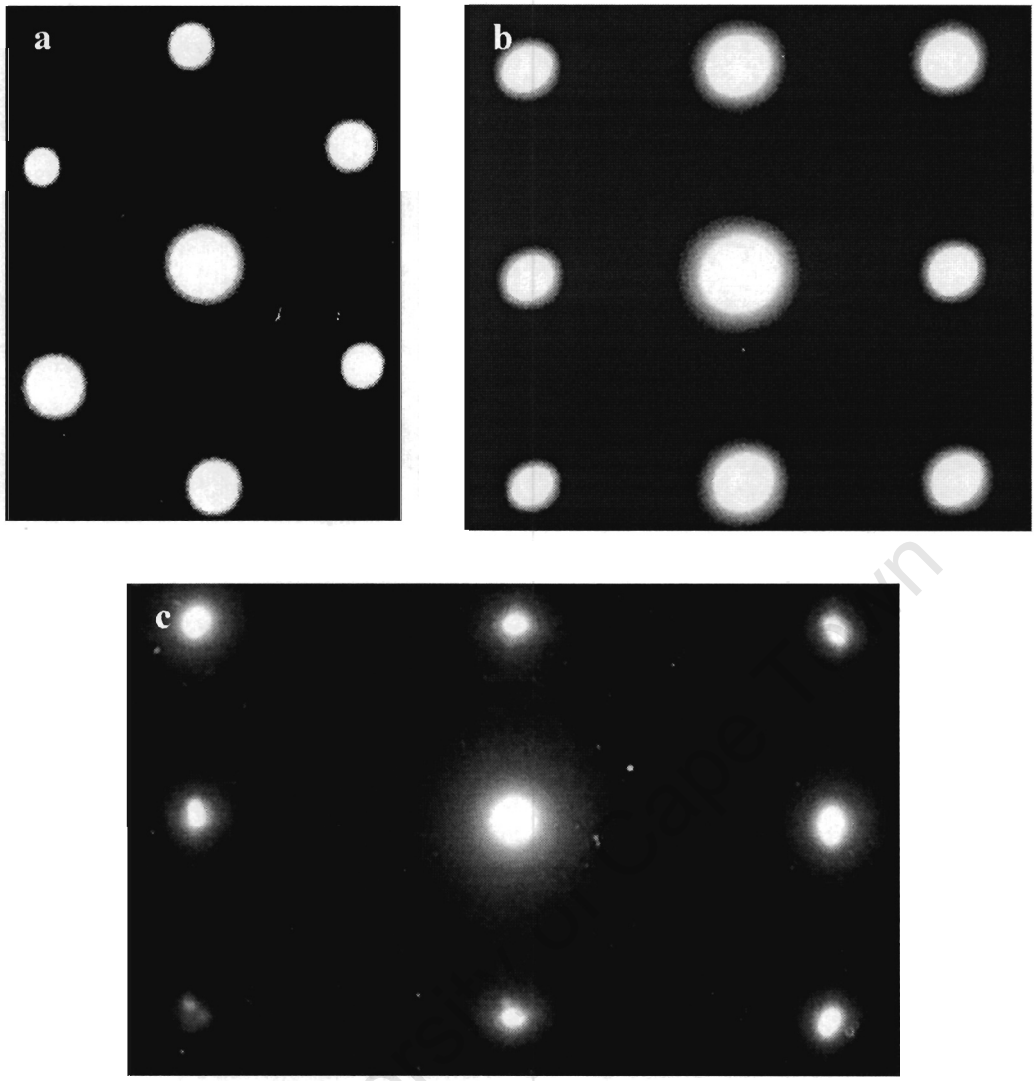

Figure 4-33 Electron diffraction patterns from initially quenched Pt 14 at. % Cu after heat treatment at 500°C for 3 hours, viewed along the (a) $[011]_{fcc}$, (b) $[001]_{fcc}$ and (c) $[112]_{fcc}$ zone axes.

4.4.4 Electron diffraction patterns of Pt 12.5 at. % Cu after heat treatment

Electron diffraction patterns of initially cold worked Pt 12.5 at. % Cu after heat treatment at 200°C are shown in this section. Figure 4-34 shows the electron diffraction patterns of initially cold worked specimens after heat treatment at 200°C. They are indexed as viewed along the $[011]_{fcc}$, $[103]_{fcc}$ and $[112]_{fcc}$ zone axes. The electron diffraction patterns for Pt 12.5 at. % Cu and Pt 14 at. % Cu appear to be the same, indicating that the same structure is formed at both compositions after heat treatment at 200°C.

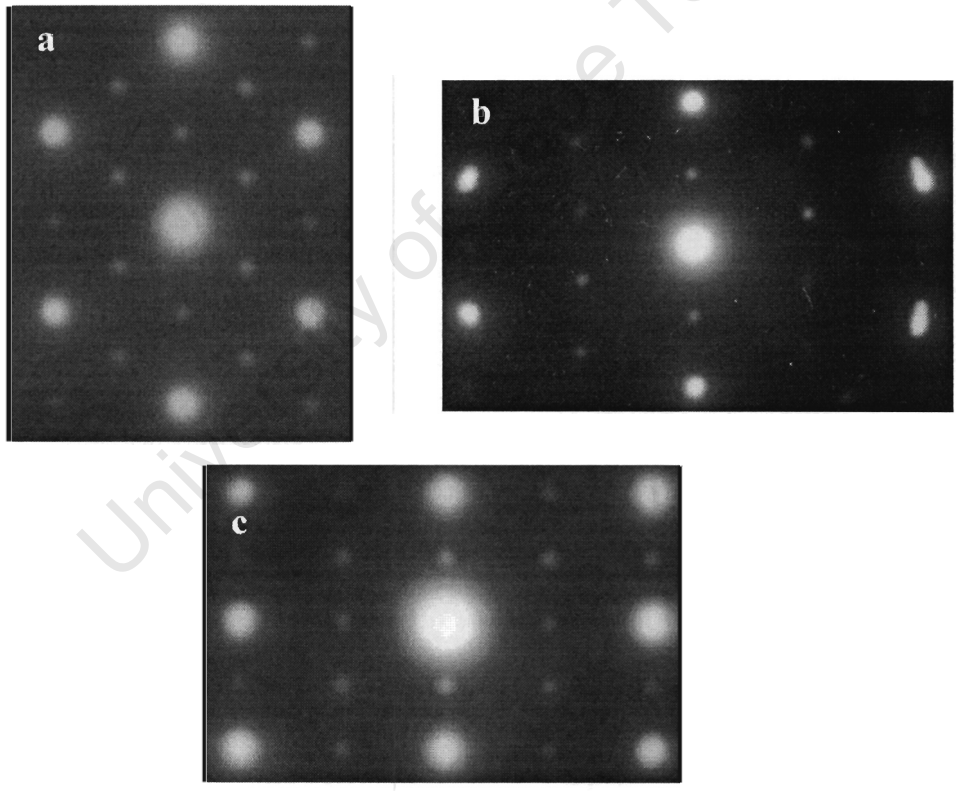

Figure 4-34 Electron diffraction patterns from initially cold worked Pt 12.5 at. % Cu after heat treatment at 200°C, viewed along the (a) $[011]_{fcc}$, (b) $[103]_{fcc}$ and (c) $[112]_{fcc}$ zone axes.

4.5 SIMULATION OF THE $CuPt_7$ STRUCTURE

4.5.1 SIMULATION MODEL AND SIMULATED ELECTRON DIFFRACTION PATTERNS

In order to determine whether electron diffraction patterns seen after heat treatment for Pt 14 at. % Cu and Pt 12.5 at. % Cu are consistent with the structure proposed by Tang[24], a model structure was simulated using JSV1.08 Structure Viewer Software Program (www.jcrystal.com/steffenweber/JAVA/JSV/jsv.html). The simulation program requires input of the lattice parameters, the space group number and the atomic positions occupied by all the atoms in one unit cell. The value for a_0 was measured by x-ray diffraction to be 3.775 Å, hence the lattice parameter of this cubic unit cell was $2 \times a_0$, i.e. 7.55 Å.

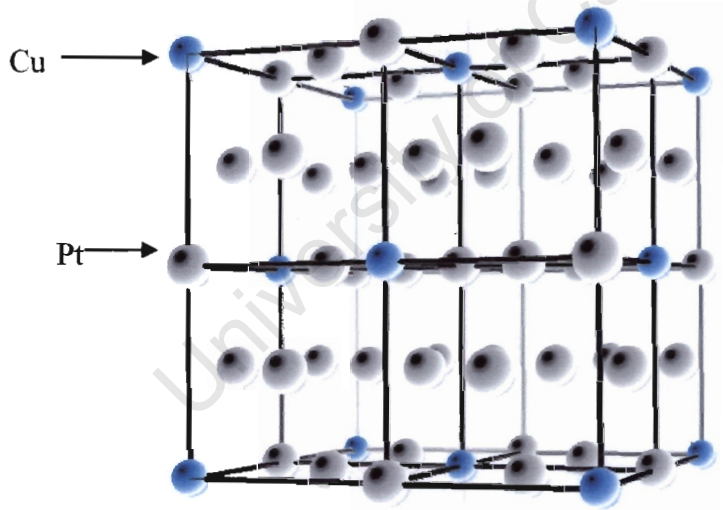

Figure 4-35 Simulated $CuPt_7$ structure, where Pt atoms are grey and Cu atoms are blue.

4.5.2 COMPARISON OF SIMULATED AND EXPERIMENTAL DIFFRACTION PATTERNS

A comparison of experimental electron diffraction patterns and simulated electron diffraction patterns were carried out. Since the same electron diffraction patterns were observed for initially cold worked and initially quenched Pt 14 at. % Cu after heat treatment below 500°C, only one set of electron diffraction patterns is compared to the simulated electron diffraction patterns. The experimental electron diffraction patterns were taken from initially quenched Pt 14 at. % Cu after heat treatment at 300°C, previously showed in Figure 4-31.

The experimental pattern in Figure 4-36a is viewed along the $[001]_{fcc}$ zone axis and is identical with the simulated pattern in Figure 4-36b, also viewed along the $[001]_{fcc}$ zone axis. Simulated and experimental electron diffraction patterns viewed along the $[112]_{fcc}$, $[103]_{fcc}$ and $[011]_{fcc}$ zone axes are also consistent, as seen in Figure 4-37, Figure 4-38 and Figure 4-39 respectively.

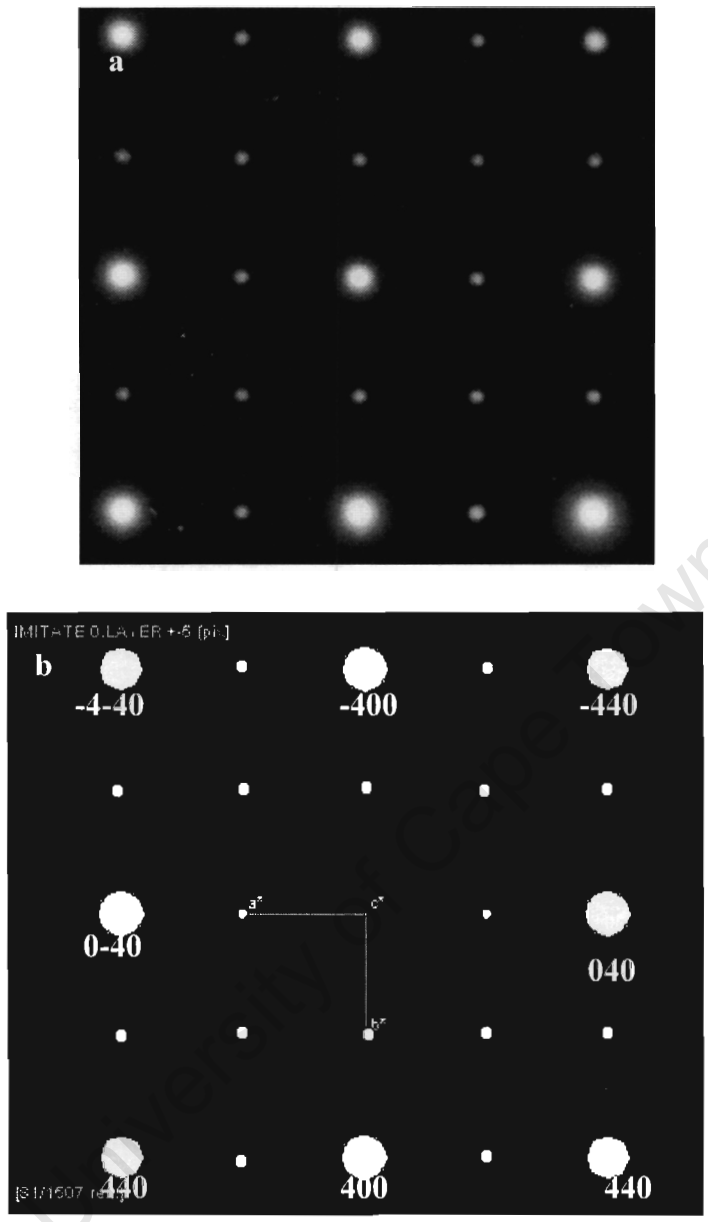

Figure 4-36 (a) Experimental electron diffraction pattern of initially quenched Pt 14 at. % Cu after heat treatment at 300°C for 3 hours and (b) Simulated electron diffraction patterns viewed along the $[001]_{fcc}$ zone axis.

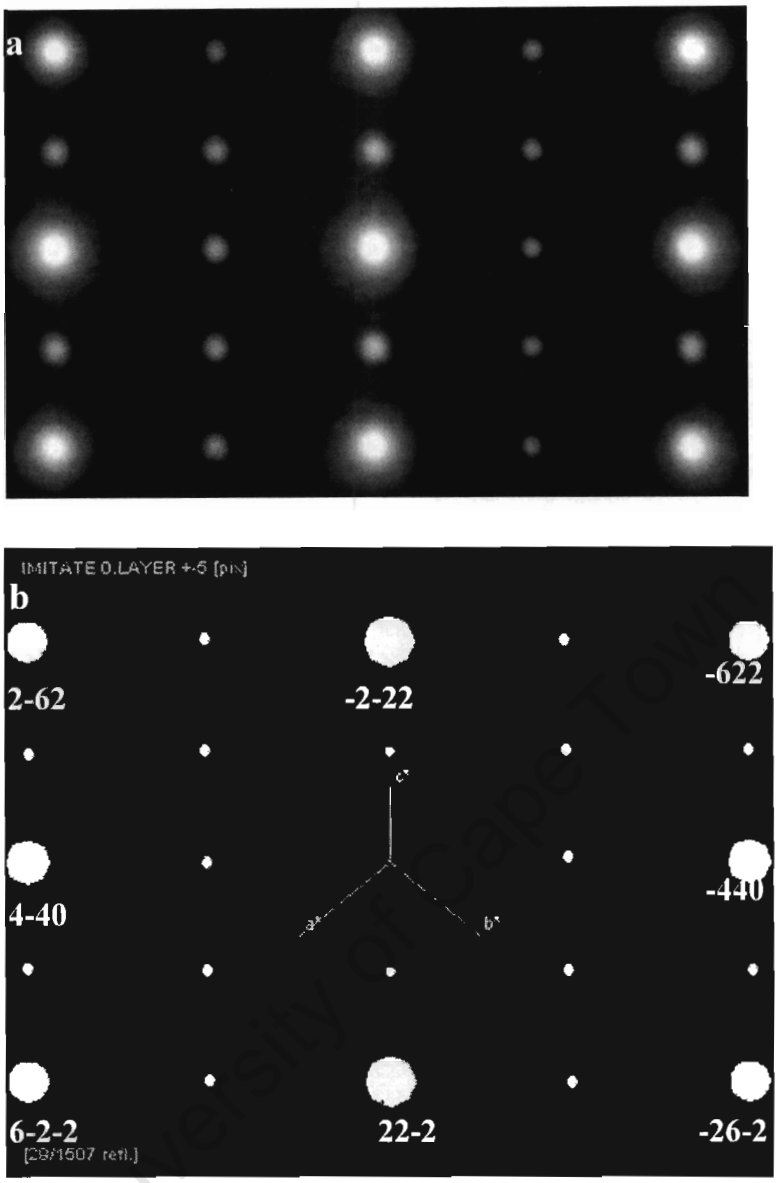

Figure 4-37 (a) Experimental electron diffraction pattern of initially quenched Pt 14 at. % Cu after heat treatment at 300°C for 3 hours and (b) Simulated electron diffraction patterns viewed along the $[112]_{fcc}$ zone axis.

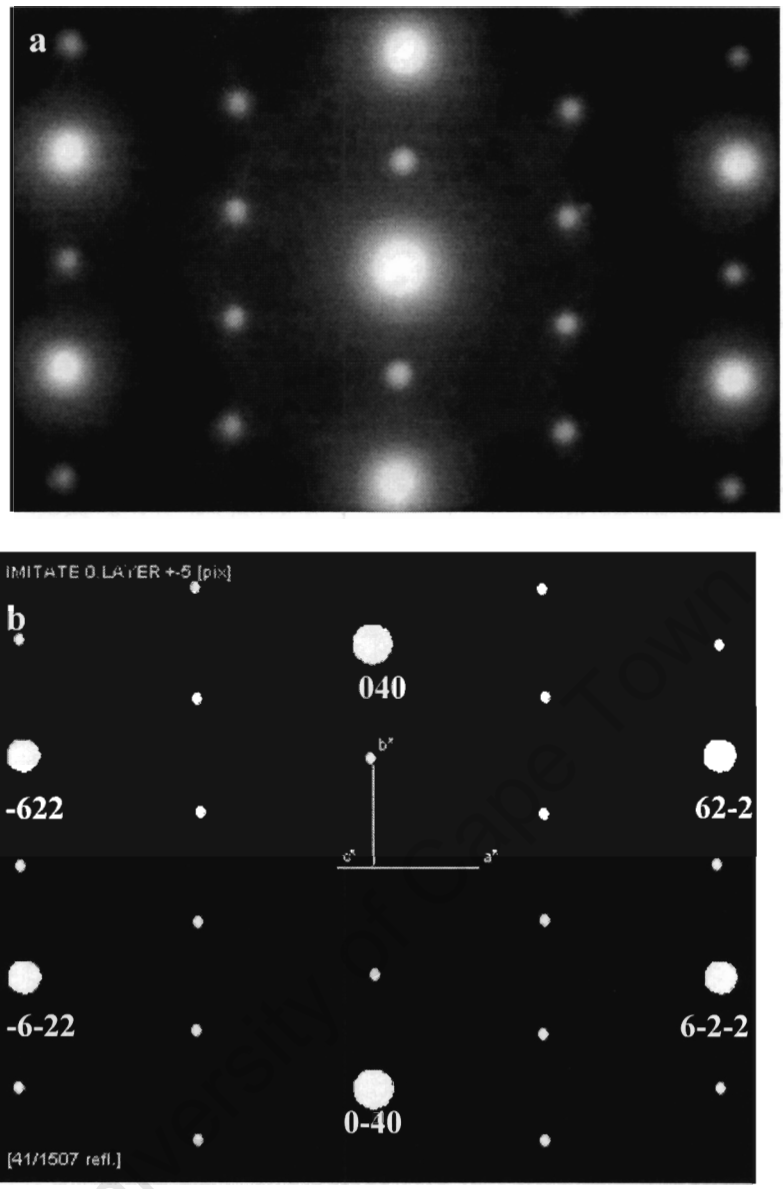

Figure 4-38 (a) Experimental electron diffraction pattern of initially quenched Pt 14 at. % Cu after heat treatment at 300°C for 3 hours and (b) Simulated electron diffraction patterns viewed along the $[103]_{fcc}$ zone axis.

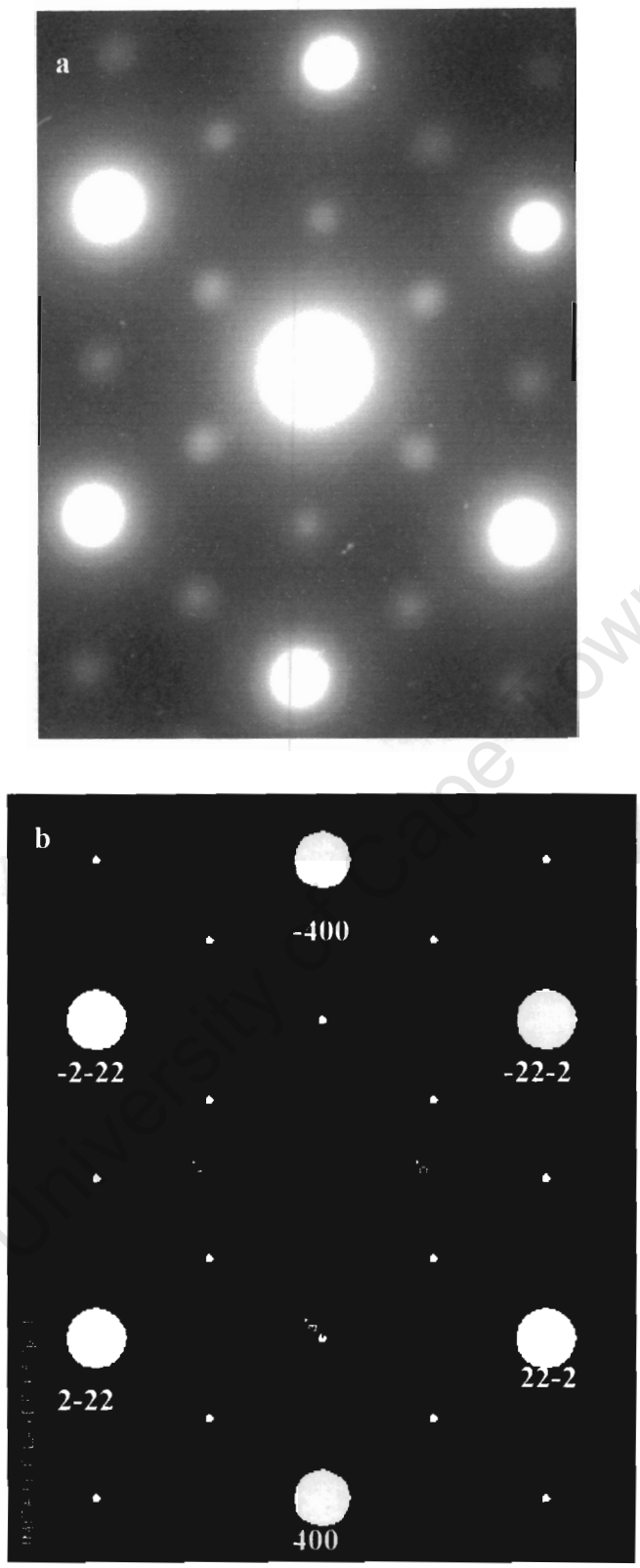

Figure 4-39 (a) Experimental electron diffraction pattern of initially quenched Pt 14 at. % Cu after heat treatment at 300°C for 3 hours and (b) Simulated electron diffraction patterns viewed along the $[011]_{fcc}$ zone axis.

4.6 DARK FIELD IMAGING

The aim of this section is to compare the morphology of the ordered regions of initially cold worked and initially quenched Pt 14 at. % Cu specimens, after heat treatment at temperatures that showed maximum hardness. Initially cold worked Pt 12.5 at. % Cu specimens were also imaged and compared to Pt 14 at. % Cu.

A dark field image reveals regions on the specimen that contributed to the diffracted reflection in the diffraction pattern that is used to form the image. Regions in bright contrast indicate the ordered regions. All of the dark field images in this section were taken using the ½ (131) superlattice reflection viewed from the $[103]_{fcc}$ zone axis as arrowed in Figure 4-40 below.

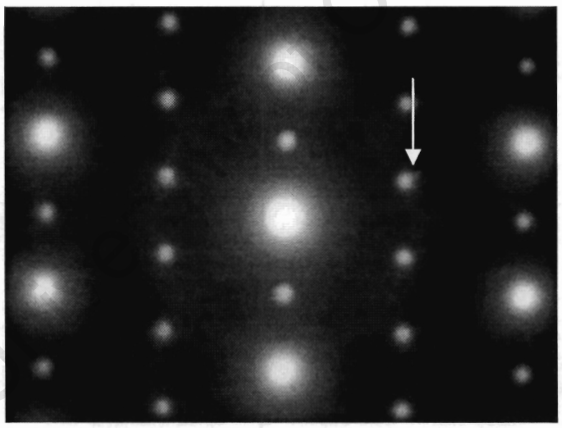

Figure 4-40 Electron diffraction pattern viewed along the $[103]_{fcc}$ zone axis and the superlattice reflection ½ (131) selected to form dark field images throughout this study.

4.6.1 DARK FIELD IMAGES OF COLD WORKED PT 14 AT. % CU

Dark field images of initially cold worked Pt 14 at. % Cu specimens were recorded and compared after heat treatment at 200°C for 3 hours, 1 week and 2 weeks.

Figure 4-41 below shows a dark field image of initially cold worked Pt 14 at. % Cu after heat treatment at 200°C for 3 hours. Ordered regions range from 5 nm to 10 nm in size. Heat treatment of initially cold worked specimens at 200°C for 1 week resulted in a structure as shown in Figure 4-42. The domain size range does not change significantly up to 2 weeks of heat treatment as shown in Figure 4-43.

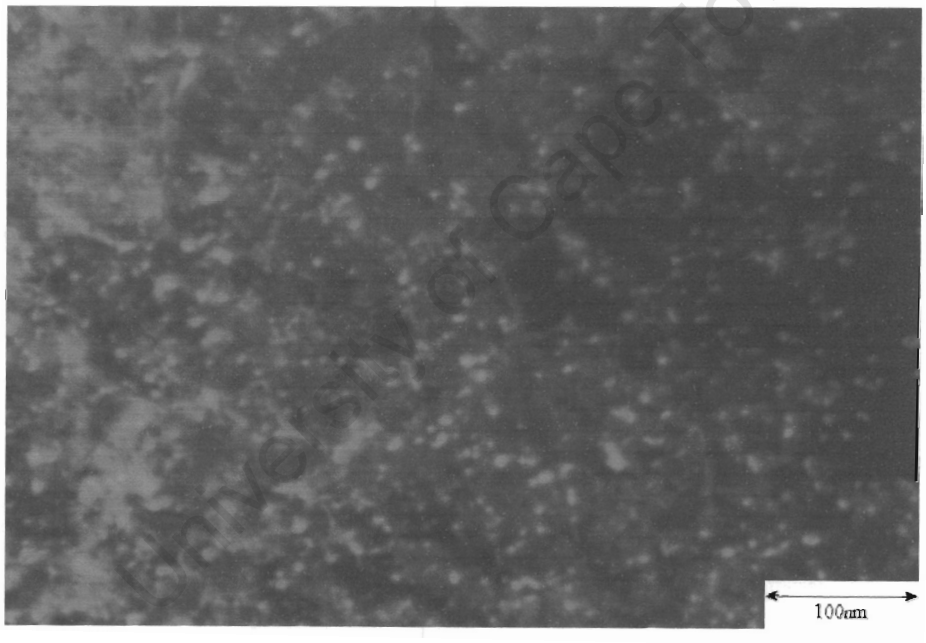

Figure 4-41 Dark field image of initially cold worked specimen after heat treatment at 200°C for 3 hours, imaged using reflection ½ (131) in $[103]_{fcc}$ zone axis electron diffraction pattern.

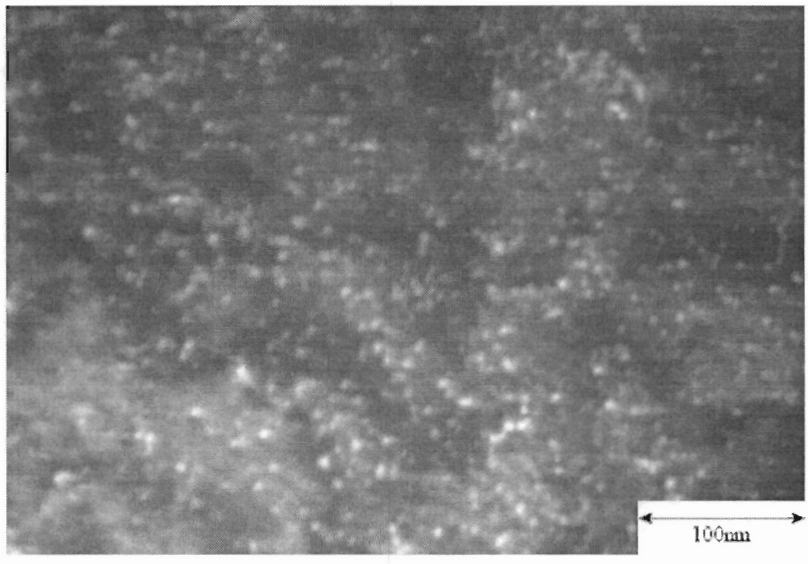

Figure 4-42 A dark field image of initially cold worked specimen after heat treatment at 200°C for 1 week, imaged using reflection ½ (131) in $[103]_{fcc}$ zone axis electron diffraction pattern.

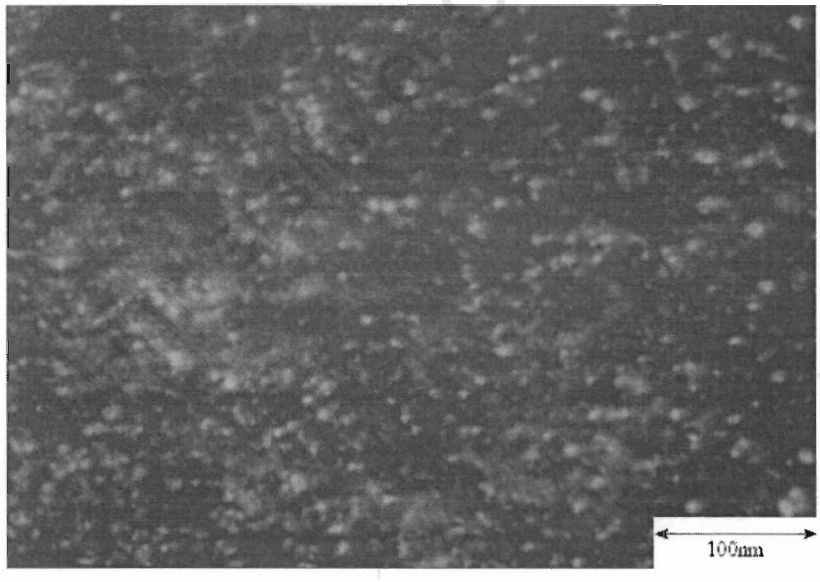

Figure 4-43 A dark field image of initially cold worked specimen after heat treatment at 200°C for 2 weeks, imaged using reflection ½ (131) in $[103]_{fcc}$ zone axis electron diffraction pattern.

4.6.2 DARK FIELD IMAGES OF INITIALLY QUENCHED PT 14 AT. % CU

Dark field images of initially quenched Pt 14 at. % Cu after heat treatment at 200°C and 300°C are shown in Figure 4-44 and Figure 4-45 respectively. Ordered regions occur uniformly throughout the sample and appear to be in the range of 15-20 nm in size for both heat treatment temperatures.

Further heat treatment at 300°C resulted in nucleation of new ordered regions. Figure 4-46 shows initially quenched specimens after heat treatment 300°C for 1 month with both small and large regions observed. Ordered regions appear to be more clustered resulting in impingement.

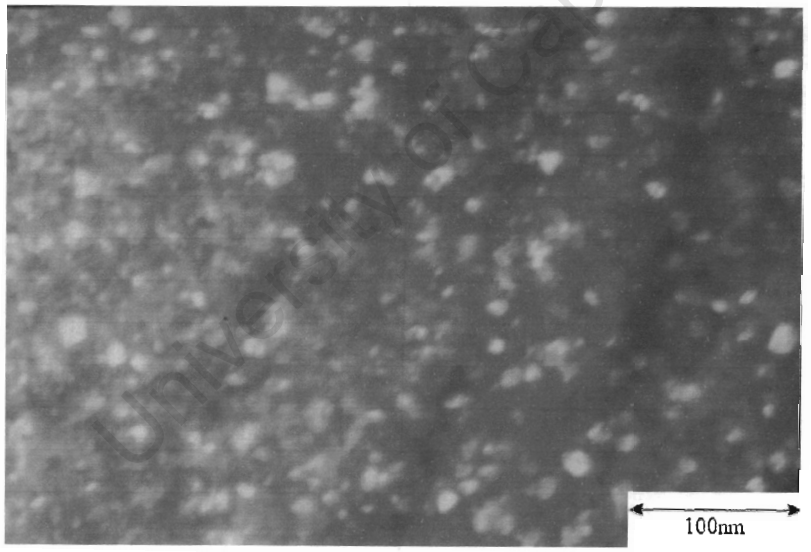

Figure 4-44 Dark field image of initially quenched specimen after heat treatment at 200°C for 3 hours, imaged using reflection ½ (131) in $[103]_{fcc}$ zone axis electron diffraction pattern.

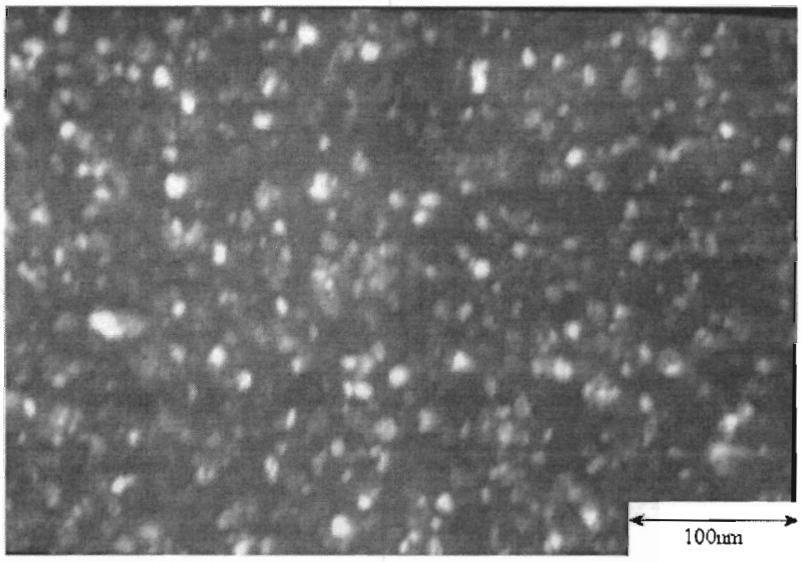

Figure 4-45 Dark field image of initially quenched specimen after heat treatment at 300°C for 1 week, imaged using reflection ½ (131) in $[103]_{fcc}$ zone axis electron diffraction pattern.

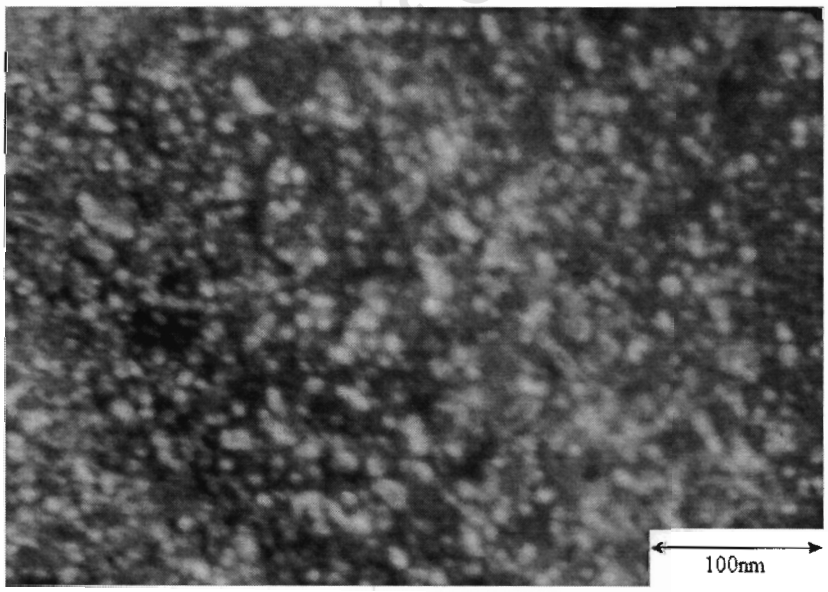

Figure 4-46 Dark field image of initially quenched specimen after heat treatment at 300°C for 1 month, imaged using reflection ½ (131) in $[103]_{fcc}$ zone axis electron diffraction pattern.

4.6.3 DARK FIELD IMAGES OF INITIALLY COLD WORKED PT 12.5 AT. % CU

Dark field images of initially cold worked Pt 12.5 at. % Cu samples after heat treatment at 200°C for 1 week, 1 month and 3 months are shown in Figure 4-47, Figure 4-48 and Figure 4-49 respectively. Dark field images show domain sizes in the range 6-10 nm, similar to that seen for Pt 14 at. % Cu. The domain size range does not change significantly up to 3 months of heat treatment.

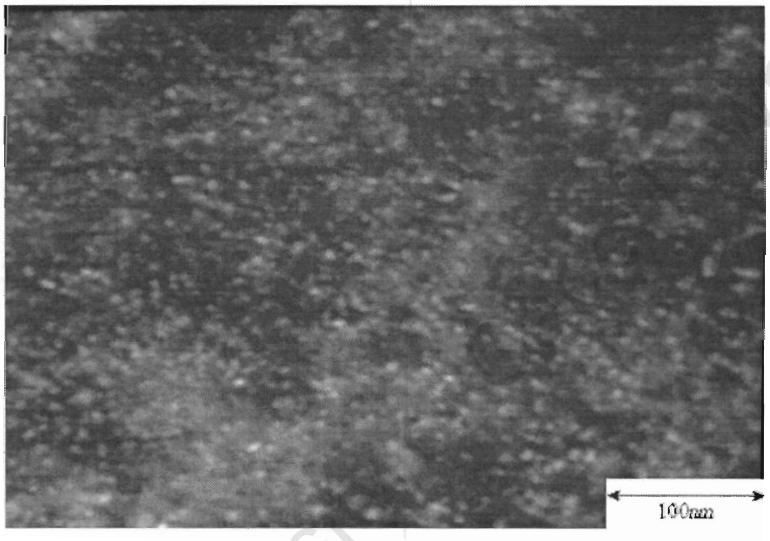

Figure 4-47 Dark field image of initially cold worked specimen after heat treatment at 200°C for 1 week, imaged using reflection ½ (131) in $[103]_{fcc}$ zone axis electron diffraction pattern.

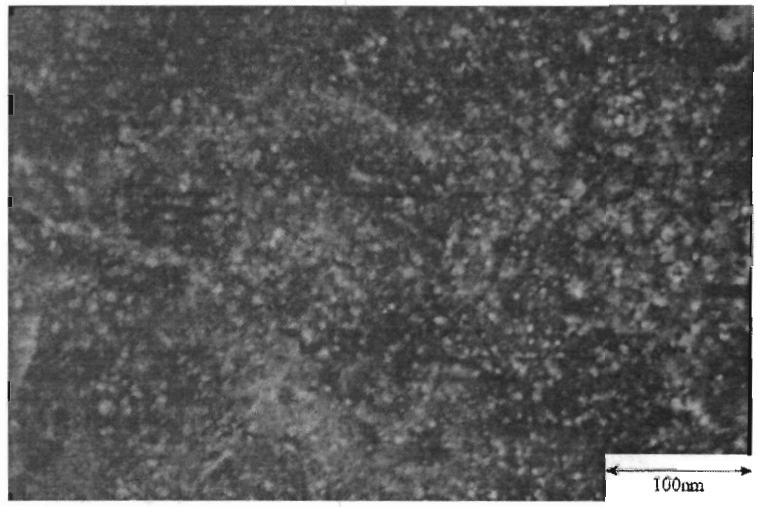

Figure 4-48 Dark field image of initially cold worked specimen after heat treatment at 200°C for 1 month, imaged using reflection ½ (131) in $[103]_{fcc}$ zone axis electron diffraction pattern.

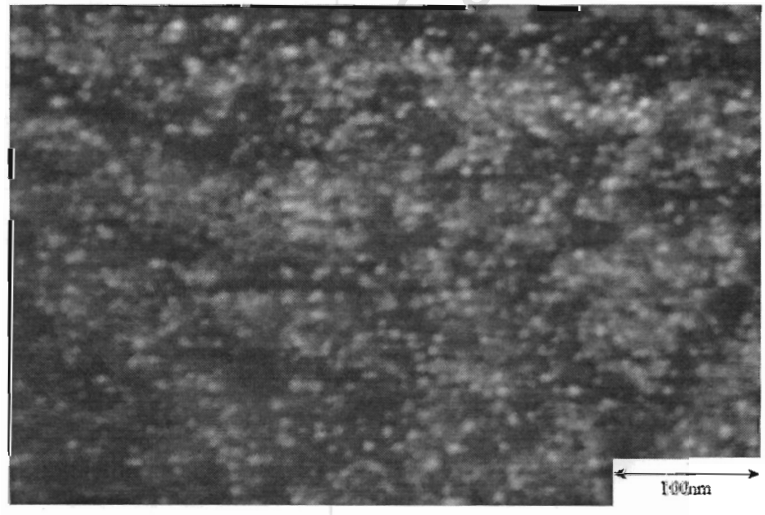

Figure 4-49 Dark field image of initially cold worked specimen after heat treatment at 200°C for 3 months, imaged using reflection ½ (131) in $[103]_{fcc}$ zone axis electron diffraction pattern.

5 DISCUSSION

Heat treatment of initially cold worked and initially quenched Pt 14 at. % Cu below 500°C results in an increase in hardness. The effect of ordering on hardness in Pt 14 at. % Cu is discussed in section 5-1. After the same heat treatment, the size of ordered regions is observed to be smaller for the initially cold worked specimens than for the initially quenched specimens. This is discussed in section 5-2. The effect of prior cold work and prior quenching on the degree of hardening in Pt 14 at. % Cu after heat treatment is discussed in section 5-3. The ordering and hardening behaviour of initially cold worked Pt 12.5 at. % Cu is compared to that of initially cold worked Pt 14 at. % Cu in section 5-4. In the last three sections of this chapter an ordering mechanism, an order type, and a hardening mechanism are proposed for Pt 14 at. % Cu.

5.1 EFFECT OF ORDERING ON HARDNESS IN PT 14 AT. % CU

Initially cold worked and initially quenched Pt 14 at. % Cu specimens showed an increase in hardness after isochronal heat treatment below 500°C. Prolonged heat treatment of initially cold work and initially quenched Pt 14 at. % Cu at 200°C and 300°C resulted in no additional increase in hardness. Results obtained from light microscopy showed no change in microstructure as a result of the same heat treatments, and XRD results were not conclusive. This type of hardening phenomenon in other alloys has been attributed to an ordering transformation occurring during the heat treatment[6,12,39].

In the transmission electron microscope, electron diffraction patterns show that an ordered structure occurs in initially cold worked and initially quenched Pt 14 at. % Cu after heat treatment at temperatures below 500°C. The structure corresponds to the cubic $CuPt_7$ ordered structure and was confirmed by comparison with the simulation in Section 4-5. Prolonged heat treatment of initially cold worked and initially quenched Pt 14 at. % Cu at 200°C and 300°C respectively showed that the $CuPt_7$ structure is stable since it was observed after one month of heat treatment. After heat treatment above 500°C, the $CuPt_7$ ordered structure was not observed.

A relationship between hardness and the formation of the $CuPt_7$ ordered structure can be inferred. Specimens that hardened after heat treatment below 500°C also exhibited the $CuPt_7$ ordered structure. After heat treatment above 500°C, the hardness decreased and the $CuPt_7$ ordered structure was not observed. The hardness increase occurring as a result of heat treatment below 500°C is therefore associated with the observed $CuPt_7$ ordering transformation.

5.2 EFFECT OF COLD WORK AND QUENCHING ON DOMAIN SIZE IN PT 14 AT. % CU

Ordering transformations can be affected by the presence of defects that generally speed up the ordering process, as discussed in section 2-4. Cold work introduces a variety of defects including dislocations and vacancies. Quenching from elevated temperatures introduces predominantly vacancies. Previous cold work and quenching of Pt 14 at. % Cu had different effects on the size of the $CuPt_7$ ordered regions formed. It is therefore assumed that the difference in defect type present before heat treatment influences the size of ordered domains which develop during heat treatment.

Excess vacancies are present in both the initially cold worked and the initially quenched specimens before heat treatment. This may be expected to enhance any diffusional transformation occurring during heat treatment. Nucleation of ordered domains appears to occur readily for both prior conditions; however, more growth of ordered domains is observed in initially quenched specimens (maximum size 20 nm) than in initially cold worked specimens (maximum size 10 nm). This suggests either that quenching results in a higher vacancy concentration than cold work, or that the vacancies in quenched specimens facilitate diffusion for longer or to a greater degree. Initially quenched specimens, however, are expected to have a lower vacancy concentration than initially cold worked specimens[15,16].

Excess vacancies in initially quenched samples appeared to continue to contribute to the ordering transformation even after the maximum domain size was reached, as shown by the nucleation of new ordered regions after heat treatment for one month. In contrast, prolonged heat treatment of cold worked samples did not result in

nucleation of new ordered regions. The enhanced diffusion observed in initially quenched specimens could be explained by a difference in vacancy lifespan between quenched and cold worked specimens. Cold worked specimens have a higher concentration of vacancy sinks in the form of defects such as dislocations. The high dislocation density after 90% cold work may be expected to lead to rapid annihilation of vacancies due to migration to nearby sinks during heat treatment. This is consistent with the rapid nucleation but very limited growth observed in initially cold worked specimens. In initially quenched specimens, the excess vacancy concentration, although lower, persists for longer leading to both domain growth and nucleation of new domains.

In initially cold worked specimens, once the excess vacancies have migrated to vacancy sinks, growth of $CuPt_7$ ordered regions is retarded and reaches only up to 10 nm. Initially quenched specimens have a lower concentration of excess vacancies, but the longer vacancy lifetime in the relatively defect-free specimens allows domains to grow up to 20 nm. The lack of further growth in initially quenched specimens does not appear to be related to a decrease in vacancy concentration (because nucleation continues to occur), and will be considered in section 5.6.

5.3 EFFECT OF COLD WORK AND QUENCHING ON THE DEGREE OF HARDENING IN PT 14 AT. % CU

The degree of hardening seen in Pt 14 at. % Cu is clearly affected by the conditions before heat treatment. Figure 4-1 shows that the increase in hardness due to heat treatment is greater for the initially cold worked than for the initially quenched Pt 14 at. % Cu, for all heat treatment temperatures. For both prior conditions, hardness does not increase further with increased heat treatment time.

Comparison of the morphology of the ordered regions in initially cold worked and initially quenched specimens after heat treatment at 200°C for 1 week shows regions in the range of 6-10 nm in size for the initially cold worked specimen, whereas initially quenched specimens showed less numerous domains in the range of 10-20 nm in size (Figure 4-43 and Figure 4-44). In general, initially cold worked specimens exhibit a high concentration of small ordered regions after heat treatment; whereas initially quenched specimens exhibit larger, less numerous ordered regions, together with smaller regions after long heat treatment times.

Small domains (< 10 nm) are observed in both initially cold worked specimens (for all heat treatment times) and in initially quenched specimens (after prolonged heat treatment, together with larger domains); however, the degree of hardening associated with these two prior conditions is very different. Large domains (20 nm) are only observed in initially quenched specimens, for all heat treatment times. A relatively small increase in hardness is consistently observed in these specimens. The smaller effect of prior quenching on hardening, relative to prior cold work, is therefore

associated with larger ordered domains. The mechanism of hardening is considered in section 5.7.

In summary:

Hardening of initially cold worked and initially quenched Pt 14 at. % Cu occurs due to an ordering transformation at temperatures below 500°C. The size of the ordered domains is significantly different for the two prior conditions. Shorter vacancy life span is a possible explanation for the smaller domain size seen for initially cold worked specimens. The larger domain size seen in initially quenched specimens is consistently associated with a low degree of hardening. It can therefore be concluded that the starting conditions determine the size of the ordered domains, and hence the degree of hardening of Pt 14 at. % Cu during heat treatment.

5.4 EFFECT OF COMPOSITION ON HARDENING AND ORDERING TRANSFORMATION

It is expected that at the stoichiometric composition $CuPt_7$ (Pt 12.5 at. % Cu), the alloy would become completely ordered upon heat treatment at temperatures that allow ordering, whereas the off-stoichiometric Pt 14 at. % Cu alloy should show a two-phase order-disorder equilibrium structure. In the present work, however, both compositions exhibit a two phase order-disorder structure even after prolonged heat treatment. A similar hardening behaviour was observed at both compositions after isochronal heat treatment (Figure 5-1) and isothermal heat treatment at 200°C (Figure 5-2). The morphology of the ordered regions for Pt 12.5 at. % Cu was also no different from the Pt 14 at. % Cu specimens after heat treatment at 200°C. While it is to be expected that specimens of similar composition exhibit similar behaviour, it is surprising that neither alloy orders fully. This will be considered further in section 5.6.

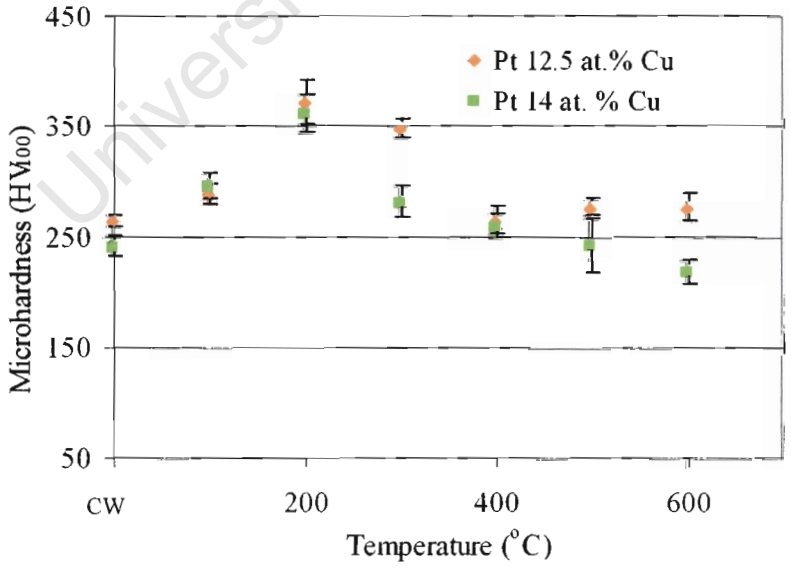

Figure 5-1 Graph of microhardness vs heat treatment temperature for initially cold worked Pt 14 at. % Cu and Pt 12.5 at. % Cu after heat treatment for 3 hours.

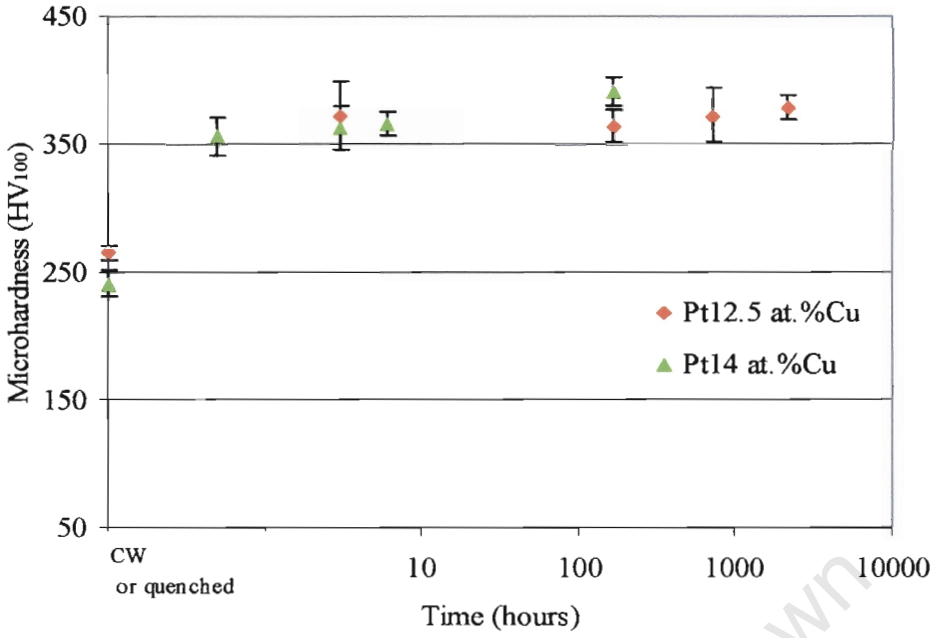

Figure 5-2 Graph of microhardness vs heat treatment time for initially cold worked Pt 14 at. % Cu and Pt 12.5 at. % Cu after isothermal heat treatment at 200°C.

5.5 PROPOSED ORDERING MECHANISM

Ordering can occur by nucleation and growth (Type I) or by a homogeneous increase in the degree of order throughout the lattice. (Type II)[2]. Type I ordering results in a heterogeneous structure whereas Type II ordering results in a homogeneous structure[2].

In Type I ordering transformations, ordered domains may nucleate at defect sites such as dislocations and vacancies. Nucleation can also occur homogeneously. In the present work, a two phase (heterogeneous) structure is observed but the ordered domains are not observed to occur preferentially at defect sites. The mechanism of ordering is therefore homogeneous nucleation of an ordered phase in a disordered matrix, resulting in a two phase structure, i.e. a Type I transformation.

5.6 PROPOSED TYPE OF ORDER

Dark field images of Pt 14 at. % Cu after heat treatment below 500°C show a heterogeneous structure in which disordered and ordered regions coexist. The alloy thus exhibits an intermediate degree of order, since it is neither fully ordered nor fully disordered, and cannot be classified as long range ordered.

Of the four models of short range order, the alloys in the present study do not exhibit statistical SRO[3], since there are well defined regions exhibiting a superlattice structure. The distribution of these ordered regions is homogeneous, with no evidence that ordered regions nucleate preferentially at the site of lattice defects, so the lattice defect model[3] is also not appropriate here.

Both the disperse SRO and the microdomain SRO models describe a heterogeneous state in which ordered and disordered regions coexist[3]. In the microdomain SRO model, there is no difference in composition between the ordered and disordered regions, which suggests that this model is appropriate for alloys of stoichiometric composition. The disperse SRO model will therefore be considered for Pt 14 at. % Cu.

Characteristics of the disperse SRO model are a heterogeneous structure of ordered regions dispersed in a disordered matrix and a maximum (limiting) domain size[3]. In the present work, the domain size in initially quenched Pt 14 at. % Cu is limited to a maximum of 20 nm in size, even when new ordered regions nucleate after prolonged heat treatment. The observed structure is therefore consistent with the disperse SRO model. (For initially cold worked specimens, growth was limited to less than 20 nm

because of reduced diffusion due to lower vacancy concentration during heat treatment.)

5.7 PROPOSED HARDENING MECHANISM

The increase hardness observed for initially cold worked and initially quenched Pt 14 at. % Cu after heat treatment below 500°C is associated with the formation of the $CuPt_7$ ordered structure. Hardening as a result of order has been shown to be dependent on the degree of order, the domain size, coherency strains or a combination of these[6,12,34,40]. This section discusses these factors and proposes a mechanism for the hardening observed in Pt 14 at. % Cu after heat treatment.

According to Stoloff and Davies[6], the degree of long range order *S* affects hardening. If *S* is small, the passage of unit dislocations creates wrong bonds which give rise to hardening. As *S* increases the dislocations begin to associate, creating superlattice dislocations, and the hardness of the alloy decreases[6]. The size of domains also affects the hardening. Small ordered domains dispersed in a disordered matrix cause hardening by the increased stress required for a unit dislocation to cut through the ordered regions. Once the ordered domains grow and come into contact, the dislocations become paired into superlattice dislocations which move through the long range ordered lattice with relative ease, and the hardness decreases. This has been reported in non-cubic superlattices such as CuPt, CuAu and CoPt upon isothermal annealing[34,41,42].

In the present work, domain size appears to be the dominant influence on hardness. In the isothermal curve of initially cold worked specimens in Figure 2-2, the hardness

is stable from 3 hours up to 720 hours of heat treatment at 200°C. A constant domain size is also observed from 3 hours up to 720 hours of heat treatment. For initially quenched specimens, the domains grow rapidly to a maximum of 20 nm and hardness remains constant even though new domains are nucleated.

The hardening behaviour observed in the present work can be explained with reference to the Stoloff and Davies[6] model. At small domain sizes (initially cold worked specimens), impediment of unit dislocations by ordered regions is probably the main strengthening mechanism. At larger domain sizes (initially quenched specimens), a lower degree of hardening could be explained by the presence of superlattice dislocations. For larger domain sizes, less energy is required to move superdislocations and the overall tendency will be for the material to harden less relative to smaller domain sizes[6].

Coherency strains may also contribute to strengthening by impeding dislocation motion[39]. These strains arise from differences in the degree of order or composition within the sample[39]. From XRD results however, it appears that coherency strains are not significant in this case since similar lattice parameters were seen before and after heat treatment of Pt 14 at. % Cu.

6 CONCLUSIONS

- The increase in hardness seen for initially cold worked and initially quenched Pt 14 at. % Cu after heat treatment below 500°C is attributed to the formation of $CuPt_7$ domains during the heat treatment.

- The smaller domain size observed for initially cold worked specimens is attributed to the higher defect density. Dislocations introduced during cold work act as vacancy sinks, hence reducing diffusion and limiting growth of ordered regions. Initially quenched specimens have a low dislocation density, so excess vacancies persist for longer resulting in the formation of larger (and also new) ordered regions after prolonged heat treatment. The microstructure of the sample before heat treatment therefore determines the domain size after heat treatment and ultimately the hardening in platinum 14 at. % copper.

- The smaller domains which formed in the initially cold worked specimens resulted in a higher degree of hardening after heat treatment. The hardening mechanism in initially cold worked Pt 14 at. % Cu arises from impediment of unit dislocations by ordered regions in a disordered matrix. The larger domains which formed in initially quenched specimens resulted in a relatively small hardness increase after heat treatment. This is probably due to the formation of superlattice dislocations, which can move through the ordered regions under lower stress than unit dislocations.

7 FUTURE WORK

- The higher degree of hardening seen for initially cold worked specimens was explained by the smaller domain size and impediment of unit dislocations. In order to have a better understanding of the hardening mechanism for this alloy system, it is suggested that ordered specimens are deformed and examined using dark field imaging.

- Even though a stable domain size of 20 nm was achieved for initially quenched specimens after 1 month heat treatment, the microstructure still contained smaller domain sizes and it is uncertain if this is a stable structure. It is suggested that longer heat treatment times should be carried out in order to establish if this is a two phase equilibrium structure.

- It is also suggested that quenched Pt 12.5 at. % Cu (stoichiometric composition of the $CuPt_7$ structure) would be more suitable for studying the ordering kinetics, as the volume fraction of ordered regions should be much larger.

8 REFERENCES

1. C S Barrett and T B Massalski, *Structure of Metals*, Permagon Press, Oxford (1980).
2. R S Irani, Contemporary Physics, **13**, 559 (1972).
3. B Schonfeld, Progr. Mat. Sci., **44**, 435 (1999).
4. L Trieb and G Veith, Acta Metall., **26**, 185 (1978).
5. H P Aubauer, Acta Metall., **20**, 165 (1972).
6. N S Stoloff and R G Davies, Prog. Mater. Sci., **13**, 3 (1966).
7. W Pfeiler, Acta Metall., **36**, 2417 (1988).
8. M Migschitz and W Pfeiler, Mat. Sci. and Eng., **206**, 55 (1996).
9. M J Kim and W F Flanagan, Acta Metall., **15**, 753 (1967).
10. A Kulovits, J M K Wiezorek, W A Soffa, W Puschl and W Pfeiler, J. Alloys Compnd., **378**, 510 (2004).
11. F C Larche, *Dislocations in Solids*, edited by F R N Nabarro, North-Holland, Amsterdam, **4** (1979).
12. M Migschitz, A Korner, W Garlipp and W Pfeiler, Acta Mater., **44**, 2821 (1996).
13. F Ling, R S Irani and R W Cahn, Mat. Sci. and Eng., **15**, 181 (1974).
14. W Pfeiler, R Kozubski, H P Karnthaler and C Rentenberger, Acta Mater., **44**, 1563 (1996).
15. M Spanl, P Rosenkranz, W Puschl, A Korner and W Pfeiler, Mat. Sci. and Eng., **324**, 54 (2004).
16. J M Larson, R Taggart and D H Polonis, Mat. Sci. and Eng., **9**, 31 (1972).
17. S Harper, Phys. Rev., **83**, 709 (1951).
18. F S Ham, Applied Physics, **30**, 915 (1959).
19. R Reihsner and W Pfeiler, Phys. Chem. Solids, **46,** 1431 (1985).
20. H Baker and H Okamoto (eds), Binary Phase diagrams, 2nd edition, ASM International, Materials Park, Ohio (1996).
21. K Oshima and D Watanabe, Acta Cryst. A, **29**, 520 (1973).
22. N Wu, H Iwasaki and S Ogawa, Trans. JIM, **14**, 309 (1973).
23. A Schneider and U Esch, Z. Electrochem., **50**, 290 (1944).
24. Y-C Tang, Acta Cryst., **4**, 377 (1951).
25. R Miida and D Watanabe, Appl. Cryst., **7**, 50 (1974).
26. D K Saha, T Shishodo, H Iwasaki and K Oshima, Phys. Soc. Jpn.,**72**, 1670 (2003).
27. S Takizawa, Phys. Soc. Jpn., **65**, 2178 (1996).
28. A G Khachaturyan, Prog. Mater. Sci., **22**, 1 (1978).

29. M Takahashi, T Sembiring, M Yashima, T Shishido and K Ohshima, Phys. Soc. Jpn., **71**, 681 (2002).
30. B A Men and M L Katsnelson, Phys. Stat. Sol. (a), **87**, 93 (1985).
31. RG Davies and N S Stoloff, Acta Metall., **11**, 1347 (1963).
32. R G Davies and N S Stoloff, Trans. AIME, **230**, 390 (1964).
33. M J Marcinskowski and D A Miller, Phil. Mag., **6**, 871 (1961).
34. A H Cottrell, Seminar on Relation of Properties to Microstructures, American Society for Metals, Cleveland, 151 (1955).
35. P A Flinn, Trans. AIME, **218**, 145 (1960).
36. R S Irani and R W Cahn, Acta Metall., **21**, 575 (1973).
37. F Ling and E A Starke, Scripta Metall., **5**, 759 (1971).
38. L E Tanner, Acta Metall., **20**, 1197 (1972).
39. H P Aubauer and H Warlimont, Z. Metallkde., **4**, 65 (1974).
40. M P Nzula, D J Cockayne and C I Lang, J. Alloys Compnd. (2006, in press).
41. J B Newkirk, A H Geisler, D L Martin and R Smoluchowski, Trans. AIME, **188**, 1249 (1950).
42. V S Arunachalam and R W Cahn, J.Mater. Sci., **2**, 160 (1967).

A HEAT TREATABLE PLATINUM COPPER ALLOY FOR JEWELLERY APPLICATIONS

M. Carelse, K. Jackson and C.I. Lang

Centre for Materials Engineering, Department of Mechanical Engineering, University of Cape Town

The hardening of platinum rich alloys can be a great advantage to jewellery production. Unfortunately, it is not being used to its full potential because heat treatable alloys are relatively new and not all jewellers are aware of them[1]. Pt 5wt.% Cu is the most common alloy used by jewellers because of its good formability characteristics. This paper examines the effect of heat treatment on the hardness of Pt 5wt.% Cu and is part of a project to encourage jewellers to try this method in jewellery manufacturing.

The hardening behaviour of heavily cold worked Pt 5wt.% Cu specimens was compared to specimens quenched from 1000°C after both were subjected to a systematic series of heat treatments. Annealing of quenched specimens did not result in any significant change in microhardness as shown in Fig. 1. However, a maximum increase in hardness from HV240 to HV351 was obtained after annealing previously cold worked specimens at 200°C for 3 hours (Fig. 1). Furthermore, the ultimate tensile strength (UTS) increased from the initially cold worked value of 750MPa to 920MPa after annealing at the same temperature (Fig. 1).

Specimens were etched in an aqua regia solution consisting of concentrated nitric and hydrochloric acid at 50°C for 2 minutes and their microstructures were evaluated. There was no significant change in microstructure between the initially cold worked specimen (Fig. 2) and the specimen annealed at 200°C for 3 hours. The quenched specimen showed a recrystallised microstructure (Fig. 3) and also did not display any microstructural changes after annealing at 200°C.

The results show that post deformation heat treatment increases the hardness of Pt 5wt.% Cu to a greater degree than heat treatment of the quenched alloy. The reason for this is not clear but probably relates to factors that affect the diffusion kinetics of Pt 5wt.% Cu. The initially cold worked samples show the characteristic hardening profile that is seen in CuPt and the Pt 2.9wt.% Cr alloy due to ordering [2,3]. Even though there are no visible microstructural changes after heat treatment at these low temperatures, the hardness increase of the Pt 5wt.% Cu specimens indicates that some hardening transformation has occurred. The ordering transformation phenomenon is a probable explanation for the hardening behaviour of Pt 5wt.% Cu. X-ray diffraction and transmission electron microscopy will be performed to investigate this possibility further.

The financial support of the Innovation Fund is gratefully acknowledged.

References

1. http://www.pgi-platinum-tech.com/pdf/V6N5.pdf
2. Irani, R. S. and Cahn, R. W. (1973) Acta Metall. 21, 575.
3. Nzula, M. P. and Lang, C. I. (2000) Proc. Microsc. Soc. South. Afr. 30, 7.

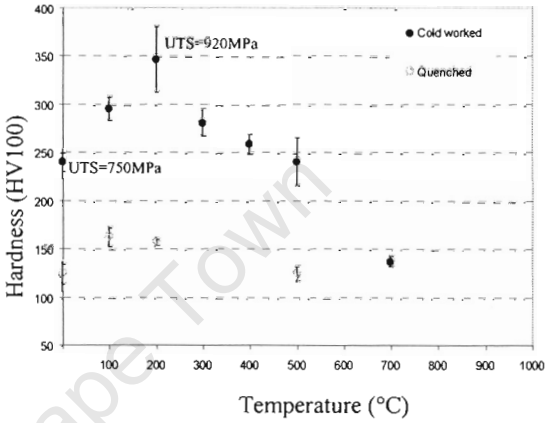

Fig. 1: Hardness graph showing effect of heat treatment temperature on the hardness of cold worked and quenched Pt 5wt.% Cu.

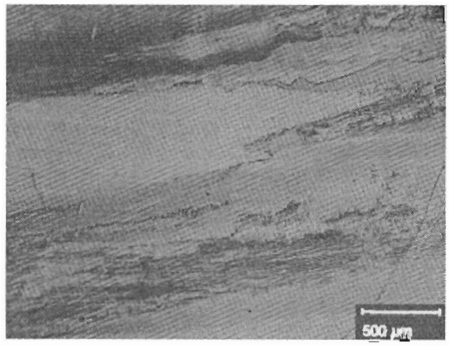

Fig. 2: Optical micrograph of Pt 5wt.% Cu showing a deformed structure after cold work.

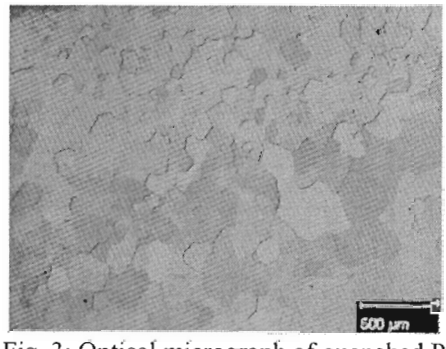

Fig. 3: Optical micrograph of quenched Pt 5wt.% Cu.